Journal of Atmospheric and Terrestrial Physics, Vol. 38, pp. 1 to 17. Pergamon Press, 1976. Printed in Northern Ireland

Equatorial electrojet and regular daily variation S_R—I. A determination of the equatorial electrojet parameters

O. FAMBITAKOYE
S.S.C. Orstom, 93, Bondy, France

and

P. N. MAYAUD*
Institut de Physique du Globe, Université Paris VI, France

(*Received* 16 *December* 1974; *in revised form* 17 *March* 1975)

Abstract—Records for 171 quiet (or almost quiet) days are available in a chain of six temporary stations and in three permanent observatories, spreading over 3000 km in latitude in Central Africa. The regular daily variation S_R is defined by the deviation from the night level in each component. In this first paper of a series investigating the properties of the variation S_R in the region of the equatorial electrojet, we describe the analysis method elaborated for determining quantitative parameters of the equatorial electrojet, and the general features of the temporal variations of these parameters.

The main principle of the analysis is an attempt at splitting up the S_R variation into two components: one of them (the S_R^E variation, E for 'electrojet') corresponds to the supplement of electric currents flowing within a narrow band along the dip equator, the other (the S_R^P variation, P for 'planetary') is the remainder of the S_R. The model used for simulating the S_R^E is tested by analyzing the current distribution of the RICHMOND (1973) model; results show that electrojet parameters obtained can be directly compared with this physical model. In order to approximate clear deformations of the magnetic profiles in some cases, the analysis is made by simulating the S_R^E with two ribbons with reversed currents. The assumption concerning the absence of an internal part in the S_R^E variation is tested. Information is given about the accuracy of the analysis.

Temporal variations of the electrojet parameters and their relation to the variation S_R^P are displayed, from hour to hour, for yearly, seasonal and monthly profiles and for two series of consecutive quiet days. The chief points coming out are as follows: (1) permanence of the counter electrojet in the morning hours and occurrence of counter electrojet events in the afternoon, (2) frequent occurrence in the afternoon of a secondary reversed current ribbon, approximately twice as wide as the main ribbon, (3) variability of the ratio of the intensities of the S_R^E and S_R^P.

1. INTRODUCTION

Many studies have been devoted to investigate the magnetic effects of the equatorial electrojet. The novelty of the present investigation consists in the quality of the data acquired during an experiment carried out in Chad and in the Central African Republic. Six temporary stations linked to three permanent observatories (see Table 1) make up a chain of nine recording points; they are located within 4° of longitude, apart of the most northern one (Tamanrasset). From November 1968 up to March 1970, the records of 171 quiet (or almost quiet) days do exist at the 9 stations.

FAMBITAKOYE (1974) gave a first detailed analysis of such data.† This series of papers sets forth the main results concerning the regular daily variation S_R of the terrestrial magnetic field, whose equatorial electrojet constitutes a particular, localized feature. In the present paper (I), we describe a method of analysis which aims at defining for each local hour of the day, quantitative parameters (centre, width, intensity) capable of simulating the electrojet; some general results concerning the temporal variations of such parameters are given. In two subsequent papers (II and III), the movements of the centre and the variations of the width and intensity are studied. In a last paper (IV), various problems raised by the magnetic profiles of particular days are set forth.

FAMBITAKOYE (1973) and FAMBITAKOYE and MAYAUD (1973) pointed out that, in the case of disturbances, the internal part of the electrojet variations is equivalent to the effects of image currents located at various depths (according to the rapidity of the analysed perturbation) but that

* Contribution I.P.G. No. 130.

† In an appendix, this thesis contains the magnetic profiles in H and Z of 171 days for each LT hour between 0630 and 1730.

Table 1. Geographic coordinates of the stations and distances from the parallel 10°N (station S_5 was moved to Bongor at the beginning of September 1969, and station S_6 to Pastor at the beginning of March 1970)

	Station	Latitude	Longitude	Distance
S1	Tamanrasset	+ 22°48'	05°31'	+ 1422 km
S2	Largeau	+ 17°56'	19°06'	+ 881 km
S3	Bol	+ 13°28'	14°43'	+ 385 km
S4	Koundoul	+ 11°58'	15°09'	+ 219 km
S5	Miltou	+ 10°14'	17°27'	+ 26 km
	(Bongor)	(+ 10°17')	(15°23')	(+ 32 km)
S6	Kotongoro	+ 08°36'	18°37'	- 155 km
	(Pastor)	(+ 9°12')	(18°37')	(- 74 km)
S7	Bouca	+ 06°30'	18°17'	- 389 km
S8	Bangui	+ 04°26'	18°34'	- 619 km
S9	Binza	- 04°23'	15°16'	-1598 km

it is very weak and practically negligible for the regular daily variation S_R. In our analysis, we assume this first result is correct; however it is put to the test again.

2. DEFINITION OF THE VALUES OF THE S_R VARIATION

The regular daily variation S_R is mainly brought about by a circulation of currents in the lower ionosphere and it is generally accepted that its amplitude is negligible during the local night. We define the amplitude of variation S_R in each component H, Z or D, at a given instant and at a given station, by the deviation in this component between the value observed at this instant and the night level.

For each day at each station, a zero level is determined by interpolating linearily between the levels of the records at a given instant, apparently quiet, of each of the nights neighbouring the day considered. Such instants are chosen within time intervals during which the level of the record is apparently constant; preference is given to quiet time intervals occurring after midnight. The same instants, in universal time, are retained at the nine stations; thus, the coherence, from one station to another, of such zero levels is guaranteed since the disturbances are synchronous in universal time, and any residual variation of the levels due to a disturbance is nearly identical at every station.

The average hourly deviations from the zero levels are scaled, from 0630 to 1730, in the three components by taking the *local* time at each station into account. Such a precaution is of importance for station S_1 only (see longitude differences in Table 1). These quantities for the three components define the hourly values of the regular daily variation S_R. Let us call them $S_R(H, x_n)$, $S_R(Z, x_n)$, $S_R(D, x_n)$ where x_n is the abscissa of a given station.

We define a quiet day by the double condition: (1) average daily Am inferior to 16, (2) average of the four 3-hr indices am between 0600 and 1800 UT inferior to 16. Monthly averages are obtained by averaging hourly values of each quiet day. Table 2 indicates the number of such days used for each month, and the average values of indices Am and FS (10·7 cm solar radiation index) for them; the total number of such quiet days is 126. We eventually use for other purposes 45 days, less quiet, since the magnetic activity condition for them is $Am \leq 24$. Seasonal averages (December solstice: D, equinox: E, June solstice: J) are derived from the average of the monthly values (November and December 1968 are not included because of the too small number of days). Yearly averages (Y) are obtained by averaging the three seasonal series of values. Because the positions of

Table 2

Month	N	Am	FS
1968			
November	3	11	133
December	3	11	149
1969			
January	8	9	157
February	5	9	156
May	5	9	145
June	7	8	158
July	16	7	147
August	8	8	163
September	8	8	148
October	14	10	161
November	10	8	151
December	8	7	136
1970			
January	13	10	152
February	9	8	179
March	9	8	144

S_5 and S_6 were shifted (see Table 1), the computation of averages D (or E) is made after reducing the monthly values observed at S_5 (or S_6) to the latitude of Miltou (or Kotongoro) by an interpolation. Similarly, the computation of averages Y is made after reducing the averages E observed at S_5 and S_6 to the latitude of Miltou and Kotongoro respectively.

3. DEFINITION OF TWO COMPONENTS OF VARIATION S_R, THE S_R^E AND THE S_R^P

Figure 1 displays, for the three components H, Z and D and for each local hour (from 0630 up to 1730), latitude profiles of the yearly values of variation S_R, such as defined above. Crosses correspond to the observed values themselves at each of the nine stations, whereas the curves are interpolated through these values by the analysis method described in Section 4.

It is obvious in Fig. 1 that the latitude variations of S_R can be divided into two components one whose latitude gradient is very rapid in the H and Z profiles only and the other whose gradient is very weak in all three components. The latter is characteristic of the magnetic effects of the confluence (and divergence) of current lines at low

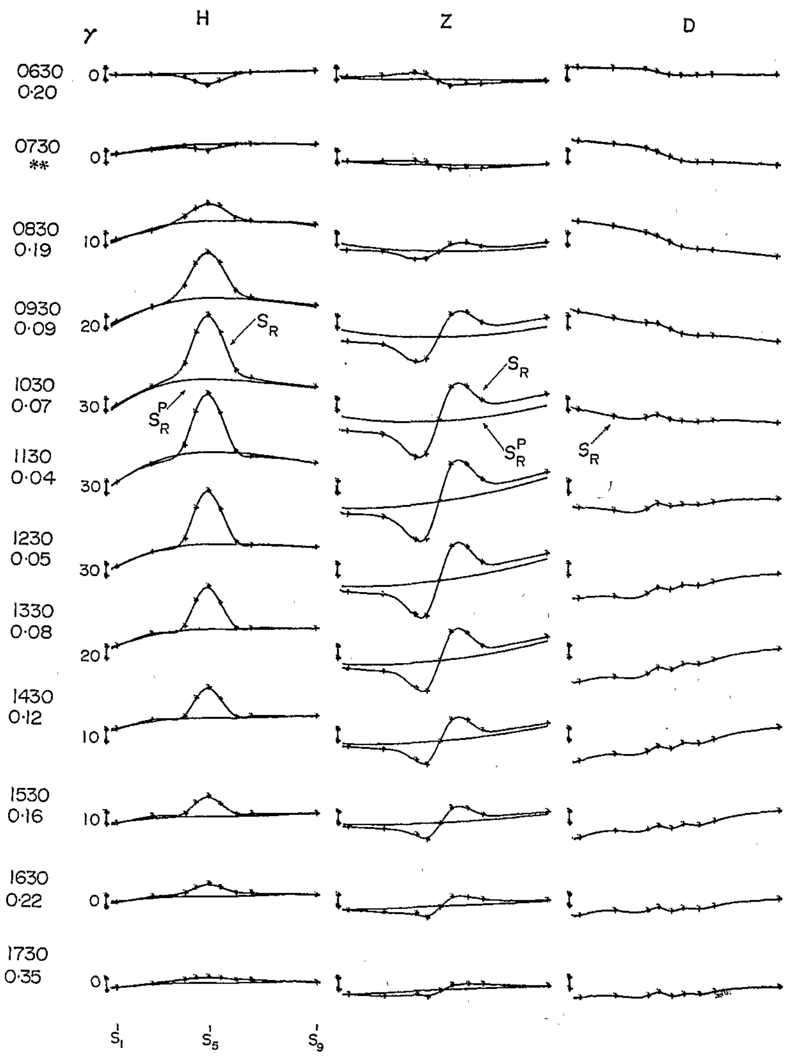

Fig. 1. Profiles of the variation S_R in H, Z and D, and of the variation S_R^P in H and Z for the year. Crosses: observed values. Scales correspond to 10 γ for the 3 components (positive towards the top). The value of the scale base is zero for Z and D, and is the indicated value for H. The number written below each local hour is the r_{18}/r_{18}' value, replaced by asterisks when higher than 0·4 (see Section 4.3 for its meaning).

latitudes of the S_R planetary vortices. The rapid variation with latitude is characteristic of the magnetic effects of a 'supplement' of currents flowing into a narrow latitude band along the dip equator (westwards at 0630 and 0730, eastwards at other hours). This 'supplement' of currents is what one calls the equatorial electrojet.

Let us call $S_R{}^E$ the part of variations S_R which corresponds to this supplement of currents (E for 'electrojet'), and $S_R{}^P$ the part which corresponds to the subjacent currents (P for 'planetary'). On Fig. 1, $S_R{}^P$ curves result from the analysis described in Section 4. The $S_R{}^E$ would thus be the difference $S_R - S_R{}^P$. One of the main efforts of this study is an attempt at carrying out a quantitative comparison of these two components.

4. METHOD OF ANALYSIS

4.1. *Fundamental principle*

Determining quantitative parameters capable of simulating the two components $S_R{}^E$ and $S_R{}^P$ is the aim of the method.

One of them, the $S_R{}^E$, is a *localized* phenomenon for which we assume that its internal part is negligible. Let us consider $P(u_1, u_2, \ldots, u_l, x_n)$ and $Q(u_1, u_2, \ldots, u_l, x_n)$ two functions expressing the magnetic effects in components H and Z at the point whose abscissa is x_n, of an external current distribution model defined by the parameters $u_1, u_2, \ldots, u_l$. Such a model would simulate the 'supplement' of currents flowing along the dip equator, and functions P and Q would simulate variation $S_R{}^E$.

The other component, the $S_R{}^P$, is a *planetary* phenomenon with external and internal parts; one cannot conceive a model of it from (or adapted to) a one-dimensional and limited profile. Then let us consider $F(f_1, f_2, \ldots, f_j, x_n)$ and $G(g_1, g_2, \ldots, g_k, x_n)$ two polynomials of x_n, expressing the magnetic effects in components H and Z at the point x_n. Such polynomials would simulate variation $S_R{}^P$.

If N is the number of points x_n where the S_R is known, one has to solve by a least-squares method the system of equations:

$$\begin{cases} S_R(H, x_n) = P(u_1, u_2, \ldots, u_l, z_n) \\ \qquad\qquad + F(f_1, f_2, \ldots, f_j, x_n) \\ S_R(Z, x_n) = Q(u_1, u_2, \ldots, u_l, x_n) \\ \qquad\qquad + G(g_1, g_2, \ldots, g_k, x_n) \end{cases} \quad (1)$$

$$n = 1, N$$

The equations are linear with respect to the unknown coefficients of the polynomials F and G, but not with respect to the unknown coefficients of the functions P and Q. Then one must linearize the equations, and the unknown coefficients are computed by successive iterations from a departure approximation.

4.2. *Choice of the functions*

4.2.1. *Functions P and Q*. Let us consider a current distribution given by the expression:

$$I(x) = I_0\left(1 - \frac{(x-c)^2}{a^2}\right)^m \quad (2)$$

$$c - a \leq x \leq c + a$$

where I_0 is the current density, at the centre c, of a ribbon whose halfwidth is a and length is infinite. The ribbon is assumed to be infinitely thin, and located at a height h of 105 km. We use $m = 2$; then the term $(x - c)/a$ rises up to the fourth degree. Let us call the distribution, in this case, a 'fourth-degree' distribution. With $m = 1$ (or $m = 0$), one would have a 'parabolic' (or 'uniform') distribution. It is of interest to note, for a comparison of our results with prior results, that when analysing magnetic effects of a fourth-degree current distribution by a parabolic (or uniform) distribution, the ratio of the widths thus obtained with respect to the width of the fourth-degree distribution is 0·82 (or 0·64).

We choose as functions P and Q the magnetic effects in H and Z due to the current distribution $I(x)$. The coefficients of functions P and Q then correspond to the three parameters I_0, a and c.

The first assumption included in the choice of functions P and Q is the absence of internal part. We shall return to that point later on (see Section 4.4).

A second assumption is the symmetrical form of the distribution $I(x)$. All present physical models of the equatorial electrojet show that the phenomenon is mainly shaped by the configuration of the lines of force of the main magnetic field. Now, although the main field at the level of the ionosphere differs a lot from a dipole field, the dip variation with latitude is linear in the narrow band (600–800 km) within which electrojet currents are flowing. This means that the shape of the lines of force is symmetrical with respect to the dip equator. Consequently the second assumption is probably reasonable. When studying the movements of the centre (paper II), we look more carefully at various small sources of asymmetry, which do exist.

About the validity of the other three assumptions included in the choice of functions P and Q (distribution law, thin layer, height chosen *a priori*), we may proceed in the following way. The numerical model of RICHMOND (1972) enables one to compute the distribution, with latitude *and* in altitude, of the 'electrojet enhancement current density'. We derive from it the magnetic effects in H and Z at points x_n (50 km apart) and we analyse the magnetic profiles thus obtained with functions P and Q. Crosses, in Fig. 2, correspond to the model values, and curves to the values computed by functions P and Q. One can also analyse (see Fig. 3(a)) the Richmond current distribution (after adding together the currents in altitude for each latitude) by fitting it with the distribution $I(x)$. Parameters I_0 and a thus obtained are practically equal (they differ by 1% only) to those obtained by the analysis of magnetic effects. Consequently, if the analysis of the observed magnetic profiles by functions P and Q leads to small residues, one can assert that the three assumptions under consideration are acceptable. Moreover, parameters I_0 and a obtained have a *physical* meaning and are *directly comparable* with the parameters derived from analyses of current distributions of the Richmond model.

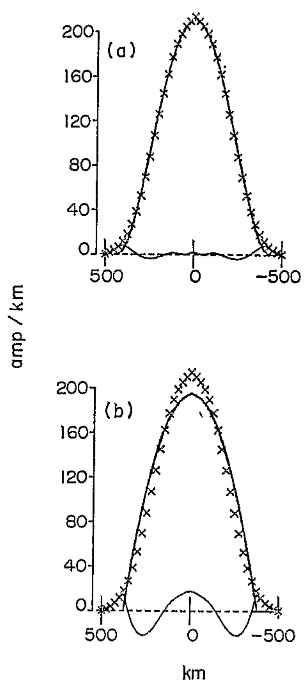

Fig. 2. Profiles of the magnetic effects of the Richmond model (crosses) and profiles of the magnetic effects of the fourth-degree model (curves) which approximate the best Richmond model effects. Profiles of residues with the same scale.

Figure 3(b) shows that the residues are greatly increased when one analyses the Richmond current distribution with a parabolic distribution $I(x)$. An analysis with a uniform distribution would be meaningless. On the other hand, when analysing the magnetic effects of the Richmond distribution with a parabolic (or uniform) distribution $I(x)$, the standard deviation of the residues is multiplied by 1·4 (or 3·1) only with respect to that obtained with a fourth-degree distribution. This means that magnetic profiles are little sensitive to a change of shape of the current distributions. Therefore any change in the shape of the observed magnetic profiles must correspond to very different current distributions.

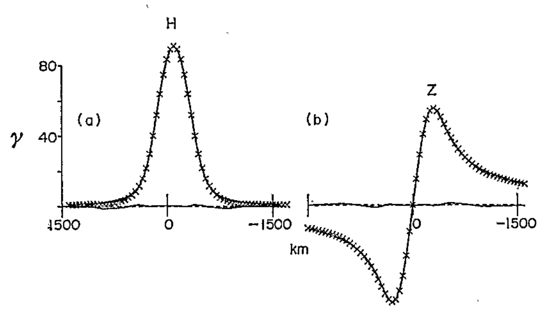

Fig. 3. Profiles of the current distribution of the Richmond model (crosses) and profiles of the fourth-degree model (a) or parabolic model (b) which approximate the best that distribution. Profiles of residues with the same scale.

In Fig. 1, the $S_R{}^E$ amplitude in H is larger at 0930 than at 1330 (and its latitude extent is wider) whereas the $S_R{}^E$ amplitude in Z is smaller (and the distance between the extremums is wider: 654 km against 542 km). One can show that the 1330 profiles are well simulated with a current distribution resulting from the superimposition of two ribbons of currents flowing in opposite directions, with the westward ribbon about twice as wide. Because such deformations of the profiles are not rare, the analysis is made with a double set of functions P and Q (assuming that both ribbons are at the same height h and have the same centre c). Consequently, unknown coefficients of functions P and Q are the current densities $I_{0,1}$ and $I_{0,2}$ (subscripts 1 and 2 refer to the main ribbon and to the secondary one) at the centre c, the half-widths a_1 and a_2, and the centre c. We indicate later on criteria by which one returns to a single ribbon when the secondary ribbon does not meet them (no attempt is made for detecting a secondary ribbon with $I_{0,1} \times I_{0,2} > 0$).

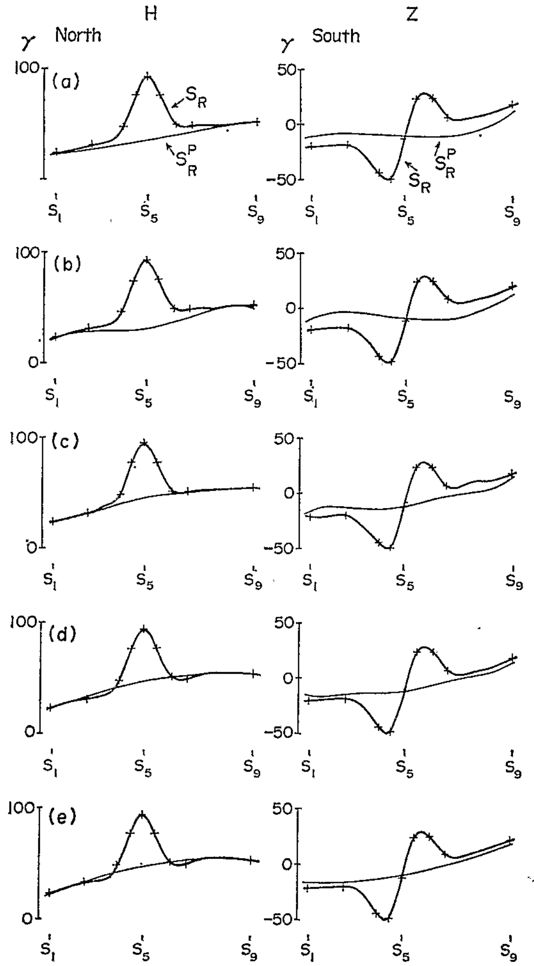

Fig. 4. Profiles of variations $S_R{}^P$ obtained by various polynomials F and G for the profiles of the S_R variation at 1230, January 1969.

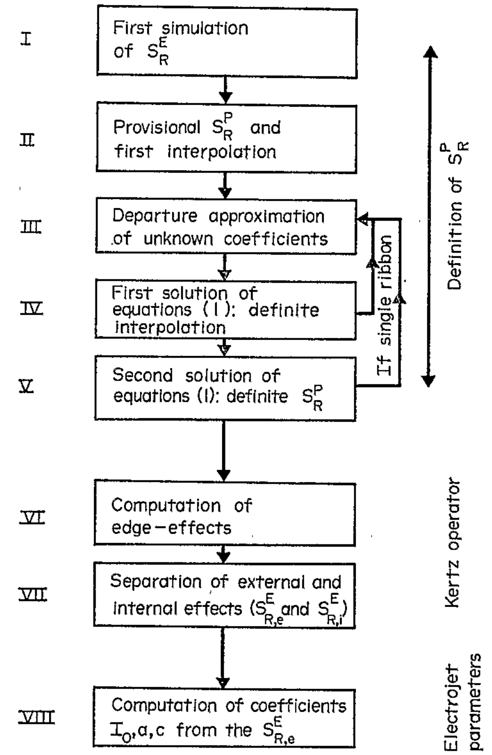

Fig. 5. Various steps and sub-steps of the analysis.

4.2.2. *Polynomials F and G.* Whereas functions P and Q simulate the $S_R{}^E$ by a current distribution which is directly comparable with a physical model, polynomials F and G only aim at simulating the $S_R{}^P$ as a 'remainder' of the S_R with respect to the $S_R{}^E$. Figure 4 shows results of various analyses made with the system of equations (1) for the *same* couple of H and Z observed profiles. In (a, b, c), functions P and Q are associated with polynomials F and G each of which contains respectively 4, 5 or 6 terms. The solutions obtained for the $S_R{}^P$ in H and Z are not stable; furthermore they undergo deformations symmetrical in H (or anti-symmetrical in Z) which do not *locally* (with respect to the dip equator) exist in variation $S_R{}^P$. One may suppress the even terms in polynomial F (except degree 0 and 2 terms, by which are simulated the broad maximum of the $S_R{}^P$ through the equatorial latitudes) and the odd terms in polynomial G (except degree 1 term for simulating the mainly linear variation of the $S_R{}^P$ through the same regions). Obtained solutions become *stable* when the number of terms used in the computation vary, but Fig. 4(d) (6 terms for each polynomial) shows that the even terms of polynomial G whose degree is high, give rise to symmetrical oscillations. The choice finally retained (terms of degree 0, 1, 2, 3, 5 for F, and 0, 1, 2 for G) is displayed in Fig. 4(e). In some cases, the natural phenomena constituted by the $S_R{}^P$ cannot be validly simulated in Z by a parabola, and residues are much higher.

4.3. *Various steps of the analysis*

Figure 5 enumerates the various steps of the analysis described in detail by FAMBITAKOYE (1974).

The first step where the system of equations (1) is solved includes an interpolation of the S_R at 63 points x_n (then, $N = 63$ in the system of equations) and the determination of the departure approximation of the unknown coefficients. A first simulation of the $S_R{}^E$ is made from its amplitude in H at the centre and from the distance between its extremums in Z (sub-step I). Then a provisional S_R^P is estimated, and a first interpolation of the S_R at four fictitious stations (two are midway between S_1 and S_2 and between S_2 and S_3, the other two are at the first and second thirds between S_8 and S_9) is made from these S_R^P and S_R^E. Finally smoothing by spline functions (REINSCH, 1967) is used for interpolating the S_R at the 63 points (50 km apart) through values observed at the nine stations and values interpolated at the four fictitious stations (sub-step II). The departure approximation of the coefficients is chosen (sub-step III). After a first solution of the system of equations (1), the interpolation is remade (as in sub-step II) by using the coefficients obtained for the S_R^E and the S_R^P (sub-step IV). Then the system of equations (1) is solved again (sub-step V). The interpolation depends on the presence or the absence of the secondary ribbon; consequently, it is remade when one chooses to make the analysis with a single ribbon (see Fig. 5) because either of the criteria described below is not met.

Values of the electrojet parameters are already available at the end of the first step. However this step is considered as a definition of the S_R^P only and the difference 'observed S_R minus computed S_R^P', considered as an 'observed S_R^E', is analysed by the Kertz operator in view of separating external ($S_{R,e}^P$) and internal ($S_{R,i}^E$) parts of the S_R^E. This second step includes a computation of the edge-effects resulting from non-zero values at the ends of the limited profiles (FAMBITAKOYE, 1973). By this step, one can check the smallness of the internal part (see discussion of Figs. 9 and 10 hereafter). Furthermore, through this operation, a smoothing of the errors of observation (*loc. cit.*) is made, which appears well by the systematic decrease (about 50%) of the amplitudes of the residues from the end of the first step to the beginning of the third one.

The definite computation of the electrojet parameters from the $S_{R,e}^E$ in the third step changes little their values; there exists a small improvement of them thanks to the smoothing mentioned above.

Two further points have to be set forth. (1) In order to avoid a secondary ribbon whose current is too small with respect to that of the main ribbon, and whose width is either too great or too small, the following criteria have to be met:

$$I_{0,2}/I_{0,1} < -a0{\cdot}15$$

$$a_1 \times 2{\cdot}75 > a_2 > a_1 \times 1{\cdot}5$$

(2) When the solution of equations (1) diverges as soon as the first iteration, this has to be considered as a failure. In other cases, the convergence is usually rapid (2 or 3 iterations), but a beginning of convergence from the departure approximation of the coefficients does not always mean that the result obtained is significant. Let us call r_{18} the standard deviation of the residues for components H and Z at the nine stations, and r_{18}' the standard-deviation of the values of functions P and Q at the same points. A small value of the ratio r_{18}/r_{18}' means that the coefficients obtained for functions P and Q well simulate the S_R^E. We choose 0·4 as the maximum value of this ratio to decide that the analysis still has a relative meaning. The high value of the limit aims at not eliminating information on electrojet parameters with evanescent S_R^E (see, for instance, profiles of 1730 in Fig. 1).

4.4. *The accuracy of the method*

4.4.1. *Analysis of theoretical values.* First of all, one can estimate the accuracy of the method by analysing theoretical magnetic effects of ribbons with given parameters I_0', a' and c', computed at the abscissae of the nine stations, and by comparing these parameters with those resulting from the analysis.

(1) Concerning the centre, even if it shifts about by more than 100 km on either side of station S_5, the parameters c and c' differ by less than 1–2 km when the value $S_R^E(H, c')$ is not too small ($>30\ \gamma$) and when the half-width is not too large ($a' <$ 500 km); the error can reach 10–20 km when $a' > 800$ km. With small amplitudes of $S_R^E(H, c')$ ($<20\ \gamma$), the error reaches up to 10–20 km.

(2) Figure 6 displays errors relative to the determination of the centre density and the width. Dashed lines correspond to parameters I_0' and a', curves to parameters I_0 and a resulting from the analysis. Level curves indicate in the domain (a', I_0') to what set of couples of values a' and I_0' corresponds a given value of the $S_R^E(H, c')$. The components of a vector such as AA' represent the corrections to be applied to a and I_0 if one interprets the differences $a - a'$ and $I_0 - I_0'$ as systematic errors. Later on, we use values without and with correction. Note that, in all the part of the domain with $S_R^E(H, c') > 30\ \gamma$, the standard deviation of the residues for the analysed profiles is about 0·2–0·6 γ.

4.4.2. *Observed yearly profiles.* The S_R^P curves drawn in Fig. 1 are those obtained at the end of the first step of the analysis. In Figs. 7 and 8, the profiles either of the $S_{R,e}^E$ and $S_{R,i}^E$ (second step),

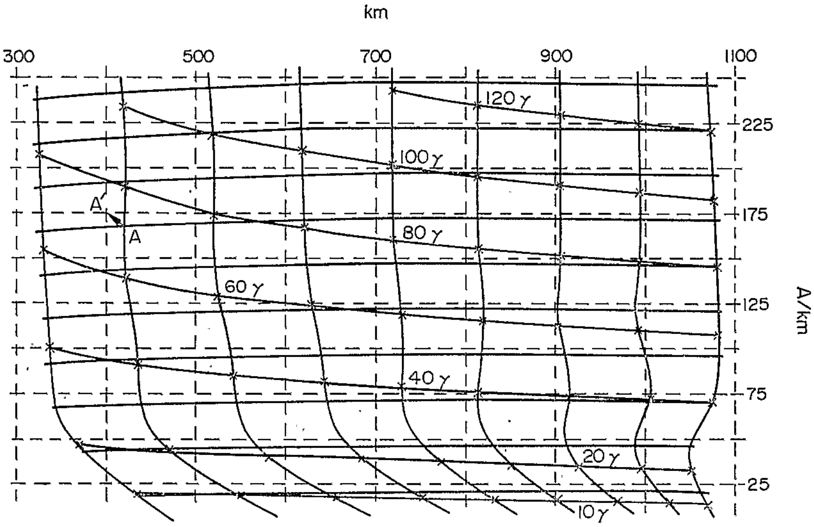

Fig. 6. Systematic errors in the determination of parameters a and I_0.

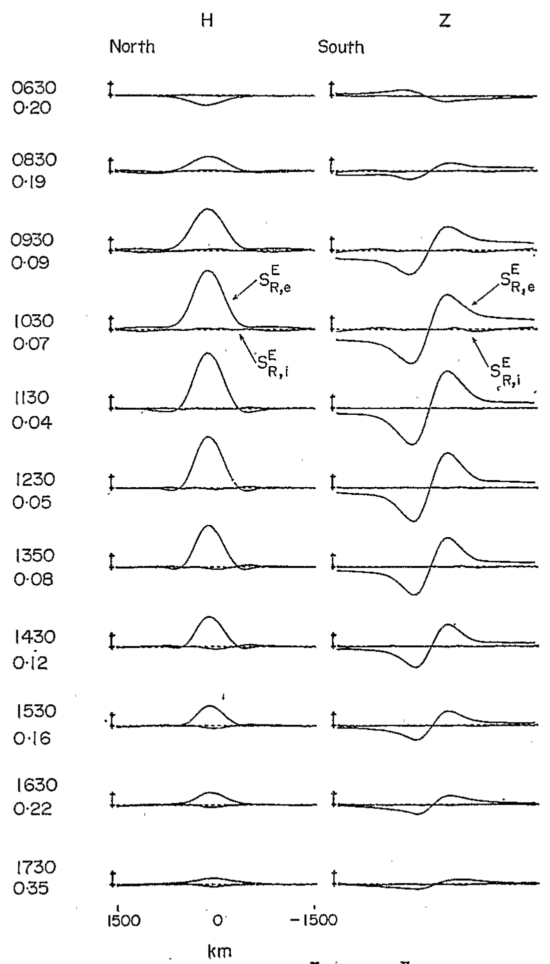

Fig. 7. Profiles of variations $S^E_{R,e}$ and $S^E_{R,i}$ for the year. Scales: 10 γ. Dashed lines: zero level.

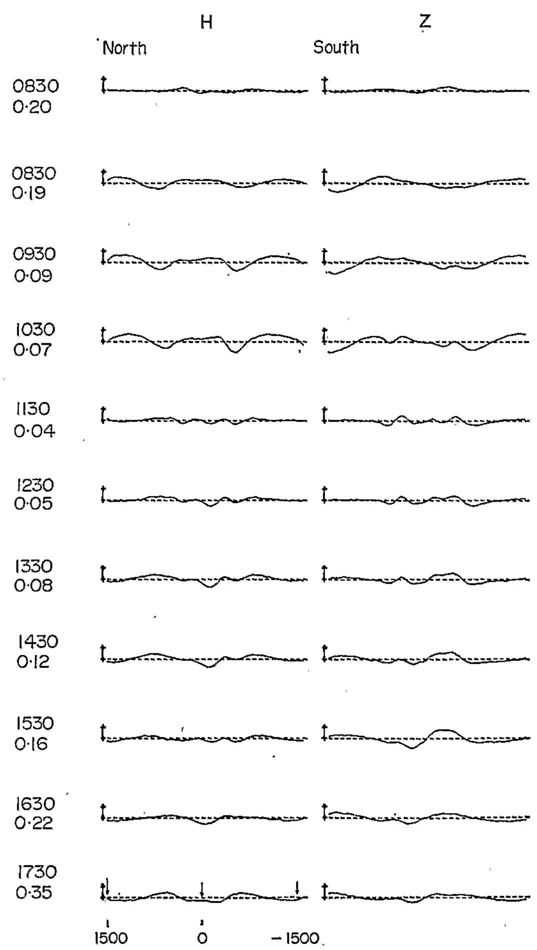

Fig. 8. Profiles of residues r, at the end of the analysis, for the year. Scales: 2 γ. Dashed lines: zero level.

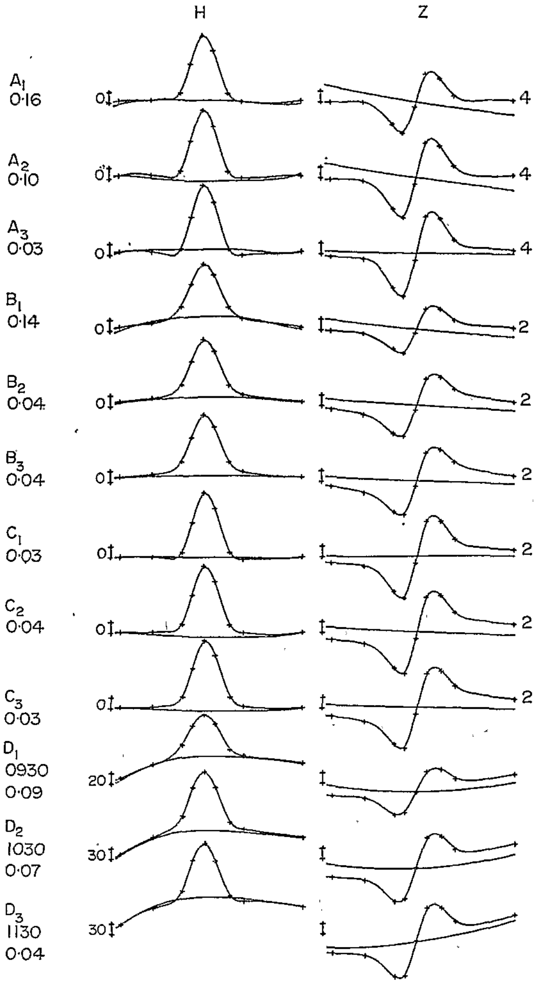

Fig. 9. Theoretical (a, b, c: see Table 3) or observed yearly (d) profiles. Crosses: computed or observed values. Scales: 10 γ. Zero-level as in Fig. 1. Integers on the right hand of computed profiles indicate the number of ribbons injected in the computation.

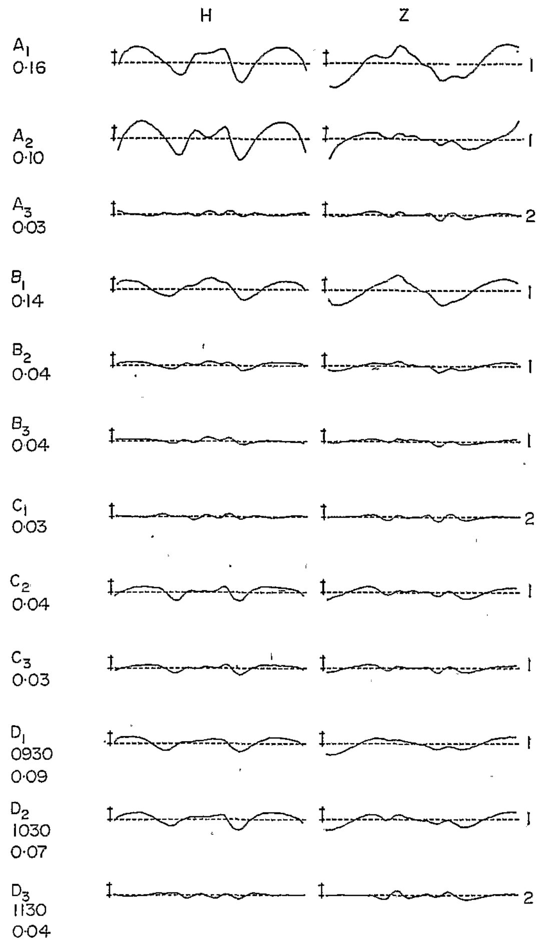

Fig. 10. Residue profiles at the end of the analysis of the profiles of Fig. 10. Scale: 2 γ. Dashed lines: zero level. Integers on the right hand indicate the number of external ribbons obtained by the analysis.

or of the residues at the end of the third step are displayed. Let us call r_{126} the standard deviation of the residues at the 63 points on components H and Z; its value is 0·9 γ at 1030 whereas it drops to 0·3 at 1130. The last value is within the range of residues obtained in analysing theoretical values (see Section 4.4.1). In order to better estimate the meaning of the residues in Fig. 8, and to check the validity of the assumption made about an absence of internal part in the $S_R{}^E$, we set forth a counter-test with Figs. 9 and 10. D profiles are identical to those of Fig. 1 at the same hours. A, B and C profiles are obtained by analysing theoretical values computed at the abscissae of the nine stations and corresponding to magnetic effects of various sets of ribbons whose characteristics are given in Table 3. In A and B, the depth of the image currents varies as does, in C, the ratio $I_{0,2}/I_{0,1}$. This ratio in A is equal to the value obtained in $D3$ by the analysis.

(1) With the theoretical profiles, the $S_R{}^P$ is null only in C_1 (see Fig. 9), the single case where the analysis detects the same number of ribbons as the number of injected ribbons. In other cases, the $S_R{}^P$ is wrong and residues become more or less large (see Fig. 10); however they are very weak in $A3$ and $B3$ because of the great depth of the image.

(2) The residues in A_1 or B_1 are considerably larger than in $D_1 - D_3$. Thus it appears that real internal effects must be substantially smaller than those due to image currents at 600 km depth.

(3) On the other hand, $D2$ resembles $C2$ and one may consider that residues in $D2$ are due to the

Table 3. Characteristics of computed S_R of Fig. 10.

	2 external ribbons	associated with	their images		
A	a_1 = 400 km a_2 = 1000 km, $I_{0,2}/I_{0,1}$ = -0.22		A1 d = 600	A2 1200	A3 1800 km
	1 external ribbon	associated with	its image		
B	a_1 = 400 km		B1 d = 600	B2 1200	B3 1800 km
	2 external ribbons a_1 = 400 a_2 = 1000 km		without image		
C		C1	C2	C3	
	$\frac{I_{0,2}}{I_{0,1}}$ =	-0.17	-0.12	-0.07	

discarding of a secondary ribbon because $I_{0,2}/I_{0,1} > -0{\cdot}15$. In $D3$ one has $I_{0,2}/I_{0,1} = -0{\cdot}21$, and a secondary ribbon is also detected from 1230 to 1530, at which hours residues are very small (see Fig. 8).

Consequently, although the internal part is partly injected into the $S_R{}^P$ by the analysis with external ribbons model final residues are sensitive to the presence of it as they are to the presence of a secondary external ribbon not detected. The smallness of the residues in Fig. 8, associated with the smallness of the $S_{R,i}^E$ in Fig. 7, shows that the differences $S_R - S_R{}^P$ in Fig. 1 are well simulated by the model (with two ribbons from 1130 to 1530). This confirms the result previously obtained for mid-day hours (FAMBITAKOYE, 1973) and extends it to other hours. Although the actual internal effects do not necessarily resemble the effects of image currents (they do in the case of perturbations—see *loc. cit.*), one can estimate from Fig. 10 that the amplitude of the $S_R{}^E$ internal part corresponds to equivalent image currents at depths larger than 1200 km.

4.4.3. *General statistics.* Table 4 gives information about the failures in the analysis, and the residues r_{126}. Failures happen either because the analysis diverges at the first iteration (A), or because the criterion $r_{18}/r_{18}' < 0{\cdot}4$ is not met (B). Besides when analysing the profiles of individual days, it happens with small amplitude $S_R{}^E$ that the centre is often determined to lie far from the dip equator (hundreds of kilometers) or that the width

Table 4. Numbers (A, B, C)—and, on the right hand, total percentages—of cases where the analysis fails; values of r_{126} or average values $\overline{r_{126}}$ with their σ's (in γ's)

	6h30	7h30	8h30	9h30	10h30	11h30	12h30	13h30	14h30	15h30	16h30	17h30	
					1 yearly profile per hour								
B	0	1	0	0	0	0	0	0	0	0	0	0	
r_{126}	0.2	-	0.7	0.9	0.9	0.3	0.4	0.5	0.5	0.6	0.5	0.5	
					15 monthly profiles per hour								
A	0	1	1	0	0	0	0	0	1	4	1	1	5.0 %
B	2	4	2	0	0	0	0	1	0	0	4	5	10.0 %
$\overline{r_{126}}$	0.3 0.1	0.4 0.2	0.9 0.3	1.0 0.4	1.1 0.4	1.0 0.4	0.9 0.4	0.7 0.2	0.8 0.2	0.6 0.2	0.5 0.1	0.5 0.2	
					171 daily profiles per hour								
A	7	13	6	1	1	1	4	5	12	18	12	23	5.0 %
B	47	52	29	14	2	2	6	12	11	22	47	61	14.9 %
C	5	4	1	0	3	1	2	1	3	2	7	22	2.5 %
$\overline{r_{126}}$	0.6 0.2	0.8 0.3	1.1 0.4	1.4 0.6	1.4 0.6	1.3 0.6	1.3 0.6	1.2 0.5	1.1 0.4	0.9 0.3	0.8 0.3	0.6 0.2	

of the main ribbon is very great. Then we had to introduce another criterion (C) defined by $|c - c_0| < 150$ km (c_0 being the average position of the centre at 20 km north of the parallel 10°N) and $a_1 < 1100$ km. With yearly profiles, r_{126} values themselves are indicated; with the others, the average r_{126} and the standard-deviation of the r_{126} values are given.

The analysis rarely fails in the middle of the day; when it does, this corresponds to S_R^E profiles whose amplitude is small as in the early morning or in the late afternoon. Failures are more frequent in the late afternoon than in the early morning; this is due to a smaller latitudinal gradient of the S_R^E during the late afternoon (compare, in Fig. 1, profiles of 1730 and 0630 which are characteristic of such a feature).

Values of the standard-deviations indicate that, even for individual days, the accuracy of the analysis in favorable cases reaches the level obtained with the yearly profiles. Analogous values for the ratio r_{18}/r_{18}' would give similar information.

5. TEMPORAL VARIATIONS OF THE EQUATORIAL ELECTROJET

Figures 11 and 12 display gross features of the temporal variations of the equatorial electrojet. In each small graph, the diurnal variation of a parameter is displayed from 0630 LT up to 1730 LT. Curves are shorter if the analysis failed at the beginning (or at the end) of the day while missing values within the day are replaced by dashed lines. Crosses indicate that a single ribbon was detected while squares mean that two ribbons were detected; in the latter case, the arrow tip indicates the value of the parameter for the secondary ribbon. A small circle (or a larger circle) around crosses or squares indicates that the ratio r_{18}/r_{18}' is superior to 0·20 (or 0·30); thus, less accurate analyses are underlined.

In Fig. 11, a and I_0 are the electrojet parameters resulting directly from the analysis while a and I_0 are the values corrected by components of vectors AA' (see Fig. 6). With c, the zero of the curves is arbitrarily chosen at 30·6 km north of the parallel 10°N (it is the value observed at 1130 for the year); with a, the zero is 400 km for the main ribbons, 800 km for the secondary ribbons. One division is equivalent to 25 km for c, 100 km (or 200 km) for the half-width a of the main (or secondary) ribbon, 100 A/km for the densities I_0.

This is the first time that temporal variations of the equatorial electrojet are displayed in so much detail. Some of them will be discussed more fully in the following papers (II and III). We state here an initial series of remarks.

(1) According to the yearly values, the centre c undergoes a diurnal variation, still appearing with seasonal or monthly values. The centre shifts southwards in the afternoon and northwards in the early morning (a time at which the counter-electrojet is almost always present—see negative values of I_0). The centre is more to the north at June solstice than at December solstice. The order of magnitude of these shifts ranges in tens of km. In paper II, we point out how various factors can explain the better part of these.

(2) The half-width of the main ribbon is about 400 km while that of the secondary ribbon is about twice this size. According to the remark made in Section 4.2.1, an analysis made with a parabolic (or uniform) model would give values of about 328 km (or 256 km) for the main ribbon. The classical value obtained by FORBUSH and CASAVERDE (1961) is larger (330 km with a uniform model, i.e. a ratio of 1·29), due to the dip gradient, less rapid in Peru than in Chad by a ratio of 1·35, which explains quite well the difference. (The variation of main field intensity is unimportant according to the Richmond model, it reduces the width by 1·5% only from Peru to Chad). In paper III, widths observed for both ribbons are compared with the Richmond model.

(3) Parameter $I_{0,1}$ (curves) mainly reflects the diurnal variation of the S_R^E. When the secondary ribbon exists, its intensity sometimes reaches one fourth of that of the main one. The most interesting feature is the nearly constant occurrence of the counter-electrojet in the early morning. Note that at 0730 (or 0830), a transition hour exists, between the counter-electrojet and the electrojet, during which period the analysis fails most of the time because of the too complex shape of the profiles. In some December solstice months, the analysis frequently fails during the afternoon: this is due to the presence of a counter-electrojet during some days of these months, resulting in profiles with the same features as the 0730 (or 0830) profiles.

Information about the intensity variation of the equatorial electrojet is completed in Fig. 12 with the aid of various more elaborate parameters.

(1) Because the width varies, parameter I_0 does not always give an exact representation of the temporal variations of the *total* current intensity flowing within the electrojet. Then, below the symbol q_E, curves indicate the *total* current

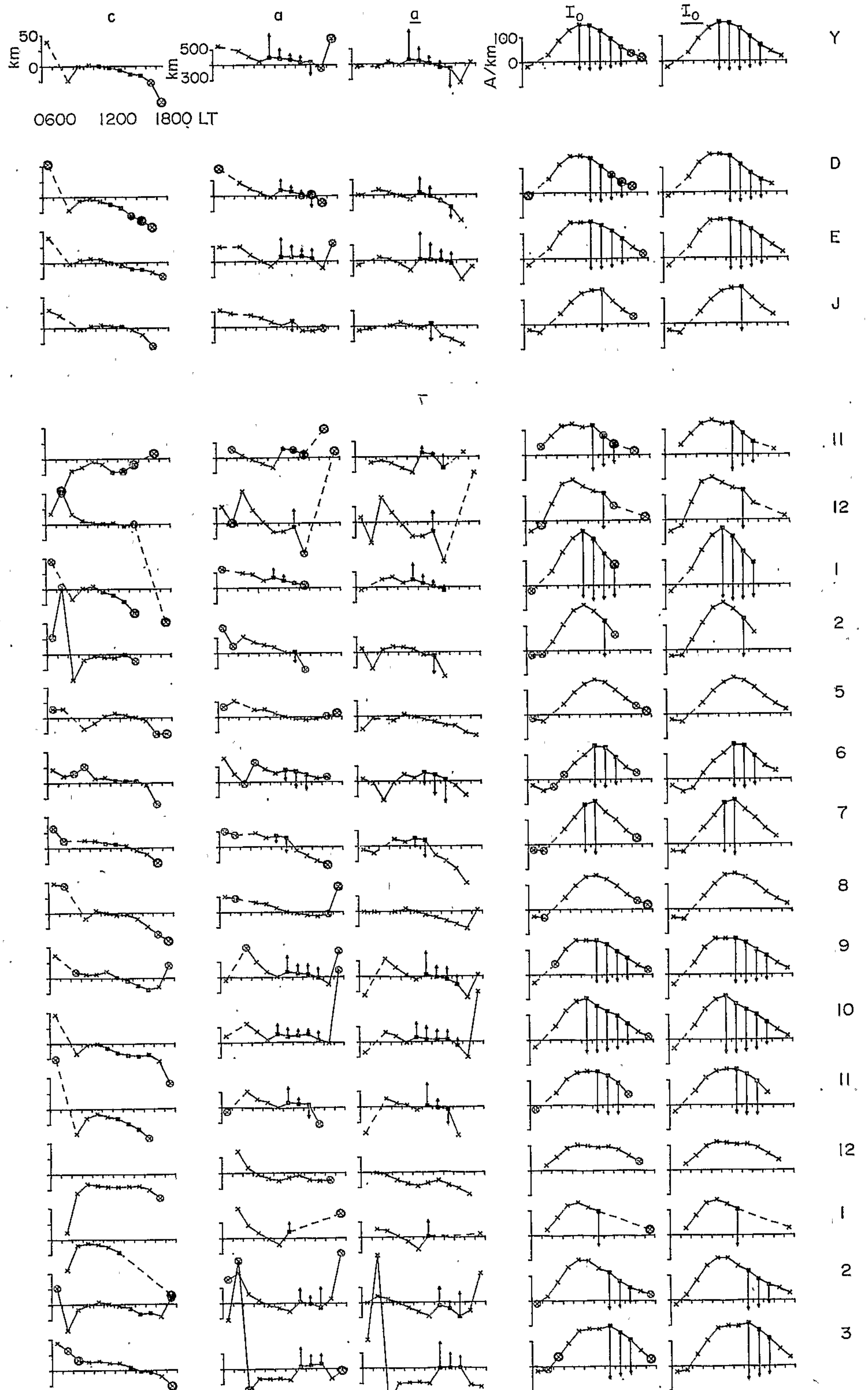

Fig. 11. Daily variation of parameters c, a and I_0 for the year, the three seasons and the months (November 1968–March 1970). Crosses: one ribbon. Squares: two ribbons. See text for other details.

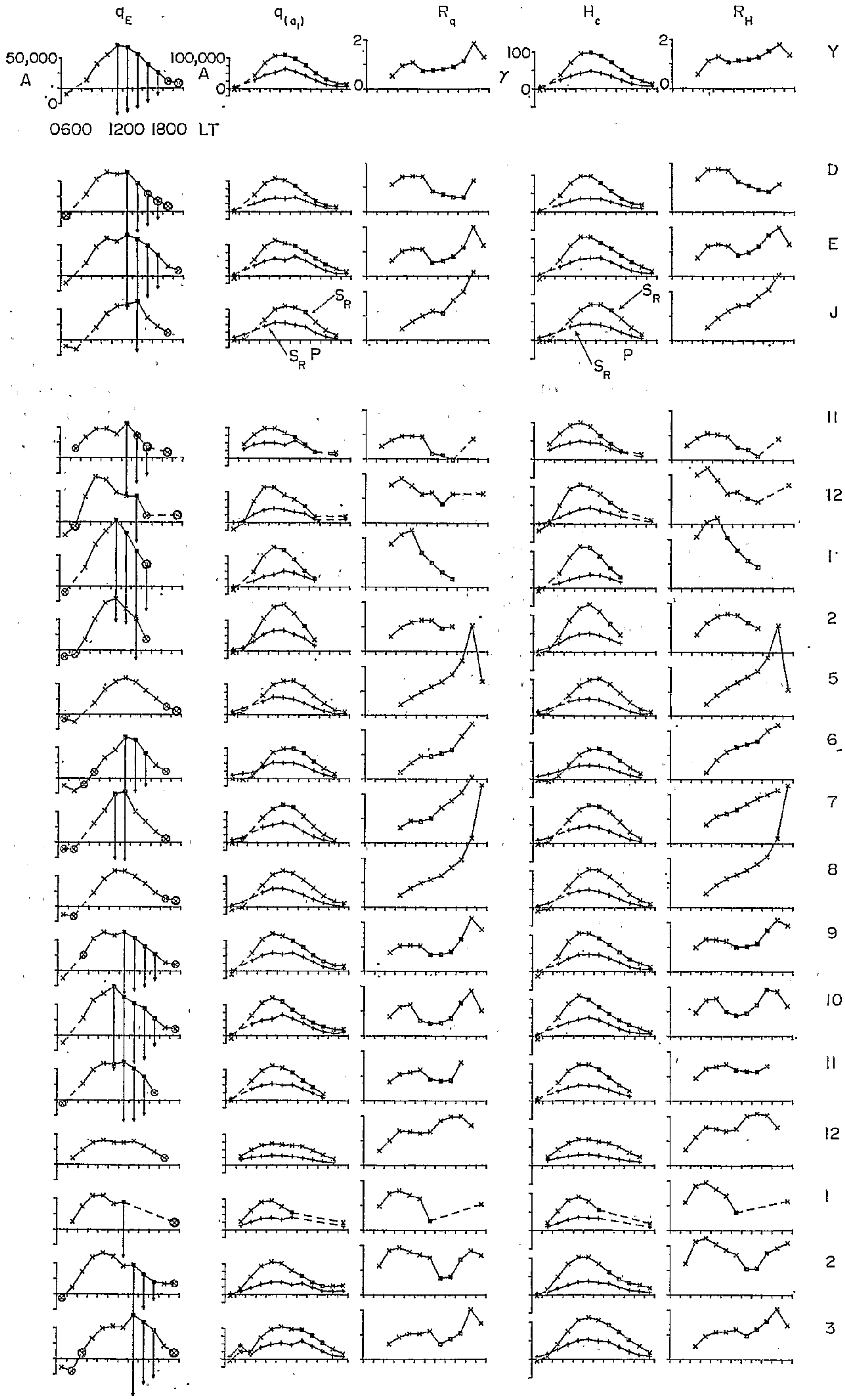

Fig. 12. Daily variation of various elaborate parameters for the year, the three seasons and the months (November 1968–March 1970). Crosses: one ribbon. Squares: two ribbons.

intensity flowing in the main ribbon (obtained by computing the integral of the distribution $I(x)$ all over the width $2a_1$); arrow tips indicate the equivalent quantity for the secondary ribbon when it exists. The chief difference with the I_0 graphs of Fig. 11 is the increased importance of the secondary ribbons with respect to the main ones, because of their larger widths. The curves themselves (main ribbon) are less regular, especially for the hourly value just before the occurrence of the secondary ribbon. Such a feature is related to an analogous feature appearing on the a curves (see Fig. 11), where a smaller width is often observed at the same time. Such a fact arises from the analysis; FAMBITAKOYE (1974) points out how, when the analysis fails in detecting a weak secondary ribbon, it causes small under-evaluation of the width of the main ribbon.

(2) $q_{(a_1)}$ and R_q curves are an attempt at a comparison of the $S_R{}^E$ and $S_R{}^P$ intensities. In $q_{(a_1)}$, the upper curve represents the total quantity of currents (in amperes) all over the width of the main ribbon (consequently equivalent to the S_R) and the lower curve represents the quantity of currents, within the same width, corresponding to the $S_R{}^P$. In R_q, the ratio of the quantities of currents corresponding to the $S_R{}^E$ and to the $S_R{}^P$ is plotted. In computing the currents corresponding to the $S_R{}^P$, we make two assumptions: (a) at each point x of the profile, we assume that the magnetic effect $S_R{}^P(H, x)$ is equivalent to the effect of a plane uniform current sheet; then the current density $I(x)$ is equal to $S_R{}^P(H, x)/0{\cdot}2\pi$ (I being expressed in A/km, and $S_R{}^P(H, x)$ in γs, (b) we retain only the external part by multiplying $S_R{}^P(H, x)$ by a factor K (let $K = 0{\cdot}72$, the value obtained by PRICE and WILKINS (1963) from an analysis of the S_q field). Then the quantity of $S_R{}^P$ currents is obtained by the integral of the function

$$I(x) = (K \times S_R{}^P(H, x))/0{\cdot}2\pi$$

from $-a_1$ to $+a_1$. For the $S_R{}^E$, currents of the secondary ribbon when it is detected are integrated over the width of the main ribbon. The $q_{(a_1)}$ curves therefore correspond to the quantity of $S_R{}^P$ or $(S_R{}^P + S_R{}^E)$ currents flowing within the interval $(-a_1, +a_1)$, whatever be the number of ribbons. Concerning the ratio R_q, since the $S_R{}^P$ currents can go to zero and even become negative (in paper IV, we point out how this can happen, especially in the late afternoon, because of small perturbations) whereas the $S_R{}^E$ currents are still non-negligible, one can have very large values (positive or negative) of this ratio. It can also happen that the $S_R{}^E$ currents become negative whereas $S_R{}^P$ currents are still positive. According to the present physical models of the equatorial electrojet (for instance, RICHMOND, 1973), $S_R{}^P$ and $S_R{}^E$ currents should be related and have the same direction. Then neither negative values of the ratio R_q nor positive values larger than 5 are plotted because, in these cases, they are the sign of a lack of connection, with respect to the theory, between $S_R{}^P$ and $S_R{}^E$ currents.

Two chief features appear in the series of $q_{(a_1)}$ or R_q graphs. Firstly, the R_q variability at a given hour from one month to another (or at a given month from one hour to another) is quite large. Compare, for instance, October and December 1969 at mid-day hours (or see August 1969). Secondly, during the morning hours, S_R and $S_R{}^P$ curves intersect whereas the $S_R{}^P$ always keeps a positive value. This means that the $S_R{}^E$ undergoes a change of sign (one already saw that from the q_E (or I_0) curves) and is apparently disconnected from the $S_R{}^P$. Examples for individual days given in Fig. 13 will stress the reality of this fact.

(3) H_c and R_H curves of Fig. 12 are analogous to $q_{(a_1)}$ and R_q curves. But, while the latter correspond to integrated values of current, the former correspond to local magnetic values. These values are based on the $S_R{}^E(H, c)$ or $S_R{}^P(H, c)$ observed (for the $S_R{}^P$, the induction factor K is used in view of selecting the external part only). The interest of such curves is their similarity with many previous comparisons between the $S_R{}^P$ and the $S_R{}^E$ (however one must take into account, for any comparison, the use of the K factor). These curves greatly resemble the $q_{(a_1)}$ and R_q curves. Note only that R_H values are systematically larger than R_q values: this corresponds to the difference between local and integrated values.

Table 5 indicates how frequently two of the special features appearing in Figs. 11 and 12 (double ribbons, counter-electrojet) occur with the individual days in relation to the classical features (single ribbon, electrojet). Similar values are given for the yearly and monthly profiles (in numbers) while percentages are used for the individual days* (see Table 4 which indicates the number of failures in relation to the 171 analyzed). When the main ribbon is a counter-electrojet (CE), it is very rare to observe a secondary ribbon. But, at 0630, the counter-electrojet is usually present

* Note that, for daily profiles, separate statistics for the 126 quiet days and the 45 less quiet days give similar percentages.

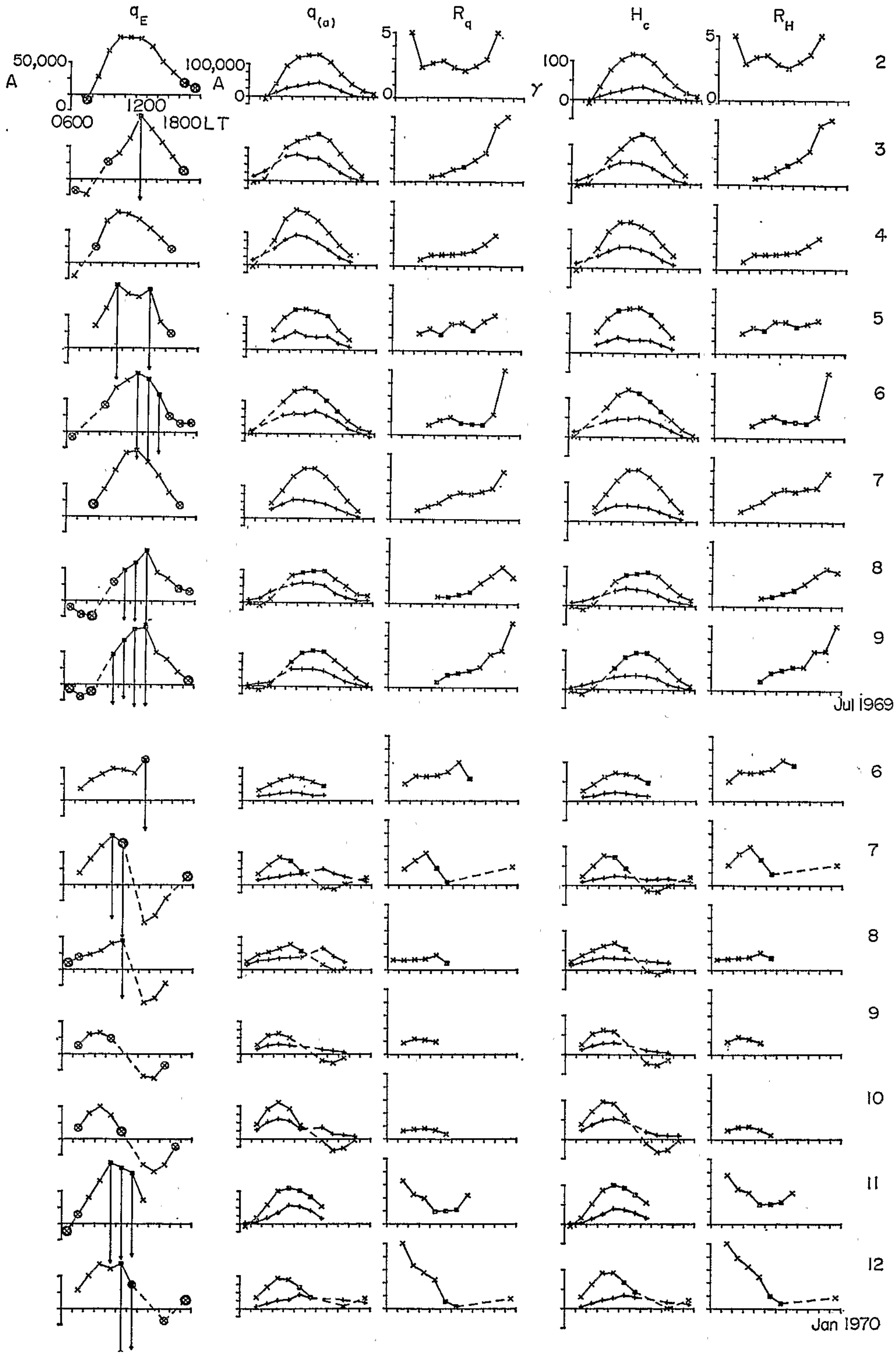

Fig. 13. Daily variation (0630–1730 LT) of various elaborate parameters for two series of consecutive quiet days (2–9 July 1969 and 6–12 January 1970). Crosses: one ribbon. Squares: two ribbons.

Table 5. Numbers (or percentages), for each hour, of normal electrojet with 1 ($E1$) or 2 ($E2$) ribbons or of counter-electrojet with 1 ($CE1$) or 2 ($CE2$) ribbons

	6h30	7h30	8h30	9h30	10h30	11h30	12h30	13h30	14h30	15h30	16h30	17h30
					Yearly profiles							
E1	0	-	1	1	1	0	0	0	0	0	1	1
E2	0	-	0	0	0	1	1	1	1	1	0	0
CE1	1	-	0	0	0	0	0	0	0	0	0	0
CE2	0	-	0	0	0	0	0	0	0	0	0	0
					Monthly profiles (numbers)							
E1	0	3	11	15	15	12	8	4	6	6	9	9
E2	0	0	0	0	0	3	7	10	8	5	1	0
CE1	13	7	1	0	0	0	0	0	0	0	0	0
CE2	0	0	0	0	0	0	0	0	0	0	0	0
					Daily profiles (percentages)							
E1	3.6	49.2	88.9	96.2	79.4	66.5	59.1	54.9	56.6	70.5	94.3	100.0
E2	0.0	0.0	2.2	3.2	20.6	32.9	40.3	41.2	35.9	18.6	1.9	0.0
CE1	93.8	47.1	8.9	0.6	0.0	0.6	0.6	3.9	7.6	10.8	2.9	0.0
CE2	2.7	3.9	0.0	0.0	0.0	0.0	0.0	0.0	0.0	0.0	1.0	0.0

(line $CE1$); it is still present at 0830. Seasonal I_0 or q_E curves of Figs. 11 and 12 show that this morning phenomenon lasts a longer time in June solstice. The counter-electrojet occurs again but much more rarely from 1130 up to 1630; it corresponds to what we call counter-electrojet 'events' for underlining the difference between the morning counter-electrojet, with almost regular daily occurrence, and the afternoon electrojet, extremely fugacious. Two further points are of interest: (a) most of these 'events' occur in December solstice (16 out of 17 events, the last one in June solstice) and they endure a few hours; even if their number is certainly underestimated (the analysis fails with small events—see Table 4, in afternoon hours), the predominance of these events in December solstice is probably *true* (see GOUIN and MAYAUD, 1967); (b) the experiment under study was made in 1968–1970, a period of solar maximum during which this sort of events is rather rare (see *loc. cit.*). The other feature appearing in Table 5 (see lines $E2$) is the frequent occurrence (up to 40%) in the afternoon of a secondary and reversed ribbon superimposed upon a main ribbon corresponding to the normal electrojet. A tentative explanation of these secondary ribbons is given in paper III.

Finally Fig. 13 gives a last illustration of the temporal variations of the equatorial electrojet. It deals with two series of *consecutive* and *quiet* (according to the double condition given in Section 2) days. Parameters displayed are those of Fig. 12 (the only difference is the change of scale for R_q and R_H). The first series (July 1969) is an example of the great variability of the ratio R_q from day to day. Compare, for instance, firstly the 2 and the 3 July, secondly the 7 and the 8 July: at mid-day hours, the ratio R_q is about 2 on the 2 or on the 7 July, inferior to 1 on the 3 or on the 8 July. One can note that the three days where ratio R_q is higher (2, 5 and 7 July) are days when the counter electrojet is weaker in the early morning. Must one assume that, in the other days, the counter electrojet is still active, although not apparent, at mid-day hours?

The second series of days (January 1970) is an example of afternoon counter-electrojet 'events.' They are present practically every day. Failures of the analysis on the afternoon of the 6 and of the 11 July mean that small 'events' are also present in these days. In graphs $q_{(a_1)}$ or H_c, crossings of S_R and $S_R{}^P$ curves are very clear and disclose, without ambiguity, the disconnection between a positive $S_R{}^P$ and a negative $S_R{}^E$.

6. CONCLUSION

In the following papers, we will undertake investigations concerning the various parameters of the equatorial electrojet and a comparison between the relative intensities of the $S_R{}^E$ and $S_R{}^P$ variations. As it stands, the proposed method of analysis provides parameters of the equatorial electrojet which are directly comparable with the Richmond model. The assumption about the smallness of the $S_R{}^E$ internal effects appears to be valid. The weakest point of the method is the incapacity of the polynomials G (a parabola) in simulating the variation $S_R{}^P$ with all its complexity; however, the residues, even for profiles of the individual days, are often very small.

Figures 11, 12 or 13 disclose, for the first time, diurnal variations of the equatorial electrojet, with the aid of various significant parameters, from day to day, from month to month, from season to season. The complexity of the phenomenon appears in full light: variability from day to day, existence of secondary ribbons, as well as permanence of the counter-electrojet in the morning hours and occurrence of it in the afternoon hours. The latter two, when a negative $S_R{}^E$ is associated with a positive $S_R{}^P$, are the sign of an apparent lack of connection, with respect to the physical models, between the electrojet and the planetary vortices.

Acknowledgements—The authors thank the Directors of Binza and Tamanrasset observatories for providing their magnetograms. Other data used in this study have been acquired with the support of Recherche Coopérative sur Programme (RCP 168) of the C.N.R.S. The authors are greatly indebted to M. VILLENEUVE, Chief of the ORSTOM Mission at Sahr (Chad), for the wonderful quality of the records in the temporary stations.

REFERENCES

FAMBITAKOYE O. 1973 *Annls Géophys.* **29**, 149.
FAMBITAKOYE O. and MAYAUD P. N. 1973 *Annls Géophys.* **29**, 168.
GOUIN P. and MAYAUD P. N. 1967 *Annls Géophys.* **23**, 41.
PRICE A. T. and WILKINS G. A. 1963 *Phil. Trans. R. Soc.* **A256**, 31.
REINSCH O. H. 1967 *Numer. Mathematik*, **10**, 177.
RICHMOND A. D. 1973 *J. atmos. terr. Phys.* **35**, 1083.

Reference is also made to the following unpublished material:

FAMBITAKOYE O. 1974 Thèse de Doctorat d'Etat, Paris VI, 28 juin 1974.
FORBUSH S. E. and CASAVERDE M. 1961 Carnegie Inst. Wash., Publ. 620.
RICHMOND A. D. 1972 *A.R.C.R.L., Rept.* 72-0668.

Journal of Atmospheric and Terrestrial Physics, Vol. 38, pp. 19 to 26. Pergamon Press, 1976. Printed in Northern Ireland

Equatorial electrojet and regular daily variation S_R—II. The centre of the equatorial electrojet

O. Fambitakoye
S.S.C.-ORSTOM, 93, Bondy, France
and
P. N. Mayaud*
Institut de Physique du Globe, Université Paris VI, France

(*Received* 30 *December* 1974; *in revised form* 2 *June* 1975)

Abstract—Magnetic ground data have previously been described, and a method for the quantitative determination of the equatorial electrojet parameters (by splitting up the regular daily variation S_R into the electrojet component S_R^E and the planetary component S_R^P) presented (Fambitakoye and Mayaud, 1975). Observed 'apparent' centres, obtained on this way, for the electrojet or the counter-electrojet, are here investigated. The actual action of various factors (asymmetry in the intensity of the total force on either side of the dip equator, shape of the dip equator on either side of the meridian of observation, asymmetry of the $S_R^P(H)$ on either side of the centre or value of the $S_R^P(Z)$) is pointed out. The 'true' centre, obtained by correcting observed values by the effect of these factors, is compared with the location of the dip equator, such as predicted by the POGO (8/69) model. For the electrojet, at mid-day hours, the 'true' centre coincides with that which we call the 'efficient' dip-equator (average location of it within a longitude sector of 30°). For the morning counter-electrojet, and, to a lesser extent, for the afternoon counter-electrojet events, the centre location is systematically about 40 km North. A tentative explanation of this deviation is given. Furthermore, one suggests that erratic locations of the centre in the early morning or in the late afternoon are due to large latitudinal gradients in the planetary S_R vortices.

In a first paper (Fambitakoye and Mayaud, 1975, hereafter called Paper I), we set forth the analysis method leading to a quantitative determination of the equatorial electrojet parameters from magnetic ground records obtained in nine stations, which make up a chain spreading over 3000 km on either side of the dip equator in Central Africa (Paper I, Table 1). By this method, the regular daily variation S_R, defined in each component H, Z and D by the deviations from the night level during quiet days, is split up into two components: the S_R^E which corresponds to the supplement of electric currents flowing within a narrow band along the dip equator, and the S_R^P which corresponds to the subjacent flow of the planetary vortices. The first component, a localized phenomenon, is determined by the means of a model for the density of currents flowing in a parallel direction with the dip equator within an infinitely thin layer located at an altitude of 105 km. The model law is defined by the expression

$$I(x) = I_0\left(1 - \left(\frac{x-c}{a}\right)^2\right)^2 \qquad (1)$$

$$c - a \leq x \leq c + a$$

where I_0 is the density at the abscissa of the centre c, and $I(x)$ is the density, at the point x, of the currents flowing within a ribbon whose half-width is a.

We here study the c parameter. However, in order to avoid any ambiguity, we call 'apparent' centre the c value obtained by the analysis. If the chosen law $I(x)$ is symmetrical, the natural phenomenon under analysis is not always symmetrical because of the various factors which we enumerate hereunder. Thus, suppose that one succeeds in showing a correlation between the 'apparent' centre variations and such factors; one can, then, apply a correction to the observed values and obtain, factor to factor and correction to correction, a new location of the centre. Let us call it the 'true' centre. The aim of the present work is to minimize the variations of the 'apparent' centre such as displayed in the first paper of this series (see Paper I, Fig. 11, left-hand column) and to compare the value obtained for the 'true' centre with the location of the dip equator.

We define the main magnetic field by the coefficients POGO (8/69). According to this model, the dip equator within the E-layer shifts southwards by 1·4 km for an altitude variation of 10 km. We choose to compute the location of it at an altitude of 105 km for the epoch 1969.5. The middle of the spell of observations is close to this time (see

* Contribution I.P.G. No. 133.

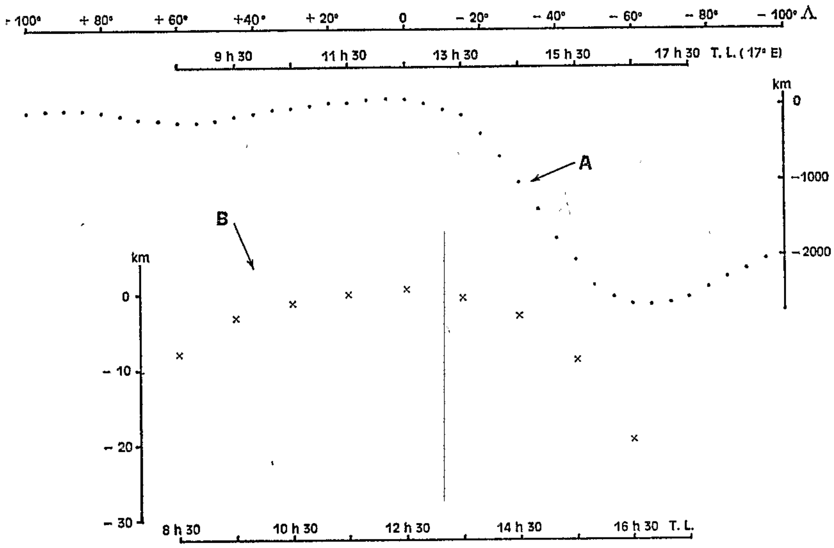

Fig. 1. (A) Location of the dip equator at 105 km height (model POGO 8/69) for 1969.5 as a function of the geographical longitude (ordinate scale in km, with respect to the parallel 10°N). (B) Values of the factor α_s (in km) as a function of the local time.

Paper I, Table 2). We use the 'apparent' centres determined from yearly, seasonal, monthly or daily profiles such as they have been previously defined (see Paper I, Section 1) for each local hour. In the case of the daily profiles, we use the whole 171 days; various trials showed that, when one retains the 126 quieter days only, the scatter of the 'apparent' centres is not significantly reduced. Recall, however, that the average profiles are obtained from these 126 quieter days only.

1. VARIOUS FACTORS LIABLE TO SHIFT THE CENTRE

The 'true' centre can be shifted by various causes: some are permanent because they are related to the main magnetic field, others are variable because they are due to variation $S_R{}^P$ which feeds the electrojet phenomenon. We call α and β respectively these two series of corresponding factors.

1.1. *Permanent factors* α

Curve A of Fig. 1 displays the 'shape' of the dip equator on either side of the meridian of our latitudinal profile, located at 17°E; the local time of this meridian is indicated by adjusting 1130 LT at the longitude 17°E. Table 1 gives, for various longitude sectors $\Delta\Lambda$ the average distances d_m of the dip equator, reckoned from the parallel 10°N.

Table 1. Average latitude of the dip equator, with respect to the parallel 10°N, for various longitude sectors centred on the meridian of observation

$\Delta\Lambda$	20°–15°	25°–10°	30°–5°	35°–0°	40°–355°E
d_m(km)	31·6	30·6	27·9	21·8	10·7

The circulation of the S_R electric currents is, at each instant, the result of a general equilibrium within the whole ionospheric layer. At 1130 LT, the electrojet reaches its largest amplitude and it can be assumed that the 'apparent' centre obtained is close to the location of the dip equator around the local meridian. Let us call 'efficient' dip equator the average location of it within a certain longitude band. At other local times, the electrojet reaches its largest amplitude at other longitudes Λ where the location of the dip equator can greatly differ (for instance, at 1430 LT, $\Lambda = -30°$E where the dip equator is 1000 km south from the parallel 10°N). The longitudinal shape of the dip equator is a first factor (say α_s) liable to cause, with local time, a variation of the location of the electrojet 'apparent' centre.

The fact which locates the 'true' centre at the dip equator is the linear dip variation on either side (2°48 by latitude degree on the 17°E), but the intensity of the total force on which the conductivities depend is not symmetrical with respect to the dip equator (it reaches its minimum at about 1000 km south) and we must induce a constant shift of the 'true' centre. Let us call α_i this second factor.

Finally a third permanent factor (say $\alpha_{s.v.}$) corresponds to the secular variation of the main field (+9·2 km according to the POGO model during the period of our observations).

1.2. *Variable factors β*

A symmetry of the equatorial electrojet on either side of the dip equator supposes a similar symmetry in the intensity of the east component of the primary electric field bringing about the variation S_R. The intensity of the $S_R{}^P(H)$ along the profile can be considered as a parameter which is approximately proportional to that of this last component. We measure its asymmetry by taking the difference between the average $S_R{}^P(H)$ value within the half-width a at the north of the 'apparent' centre, and the analogous value at the South. Let us call β_H this factor.

A non-zero value of the north component of the primary electric field is another possible source of asymmetry. Information about the intensity of the north component is given by the average value of the $S_R{}^P(D)$ over the width $2a$, whereas information about the curvature of the current lines (i.e. the longitudinal variation of the primary north electric field) is given by the average value of the $S_R{}^P(Z)$ over the same width. We call β_D and β_Z these other two factors. However β_Z is also sensitive to the latitudinal gradient of the primary east electric field and, therefore, is partly related to β_H. Furthermore, at a given time, the field direction can be eastwards ($\beta_D = 0$) but the curvature of the current lines is not null ($\beta_Z \neq 0$). Correlation coefficients between these various factors show that β_D is practically independent of β_H but somewhat related to β_Z at midday hours, whereas β_Z is more or less strictly related to β_H.

2. EVALUATION OF THE EFFECTS OF THE VARIOUS FACTORS α AND β

2.1. *The factor α_i, independent of time*

The factor α_i can be studied apart because it is the only one which is independent of time. The RICHMOND (1973) model of the equatorial electrojet does not allow the intensity of the total force F to be varied within the domain where the current distribution is computed. However one can appreciate the effect of an F variation in the following manner. Let us call F_x the value of the total force along the meridian 17°E, and $I_{0,x}$ the I_0 density which would be obtained at the centre $c = 0$ of the Richmond current distribution with a value F_x instead of the value $F_{x=c}$. We assume that, at each point x, the current density is modified by a ratio $I_{0,x}/I_{0,c}$ and we compute an assymetrical distribution such as

$$I'(x) = I_{0,x}\left(1 - \left(\frac{x-c}{a}\right)^2\right)^2. \tag{2}$$

Then we analyse this distribution by fitting it with the symmetrical distribution (1). The 'apparent' centre of the distribution $I'(x)$ is shifted southwards by 1·8 km only. The effect of factor α_i is indeed very small, and much smaller than the effects described here under.

2.2. *Factors which depend on time*

Factor $\alpha_{s.v.}$ depends on the date of the observation only and factor α_s should depend on the local time only. The effect of $\alpha_{s.v.}$ is *certainly* linear whereas we do not know the law of the action of α_s. Factors β depend on the $S_R{}^P$ for each observation. We suppose *a priori* that their effect is linear but we cannot assume that it is constant with local time.

Then, for each local hour (or group of local hours), we make a multiple linear regression analysis (BENNET and FRANKLIN, 1954) of the monthly values with the four factors $\alpha_{s.v.}$, β_D, β_H and β_Z. Factor β_D has always given a nearly null answer. Factor $\alpha_{s.v.}$ has given an answer too small, with respect to the scatter of the observations, to be considered as significant. Then we try to evaluate by the regression analysis the effects of factors β_H and β_Z only, and to estimate the effect of factor α_s as being the residual variation in local time.

Figure 2(a) displays, for each local hour (0630–1630), the variations of the 'apparent' centres obtained with the monthly and the yearly or seasonal profiles. The main fact is the difference between the location of the centre at 0630 and 0730 (counter-electrojet) and at the other hours (electrojet). We have then to deal separately with electrojet cases and counter-electrojet cases.

2.2.1. *The electrojet cases.* Table 2 gives first the average locations of the 'apparent' centres c and their standard-deviations for the monthly values by groups of three consecutive hours, then the average location $c_{H,Z}$ (and the residual standard-deviations) after the correction by a first evaluation of the factors β_H and β_Z. In each group, the standard deviation is decreasing (except in group 8, which includes 1730 LT). With groups 2–5, the c variation with local time (about 8 km) is reduced to a nearly constant value whereas a systematical variation always exists on either side.

We interpret this systematical variation as due to factor α_s. It induces a bias, within a given group, when computing the partial regression coefficients $S(\beta_H)$ and $S(\beta_Z)$. Then we assume that α_s is null at 1130 LT and, by successive iterations, we compute α_s values for other hours so that corrected values of

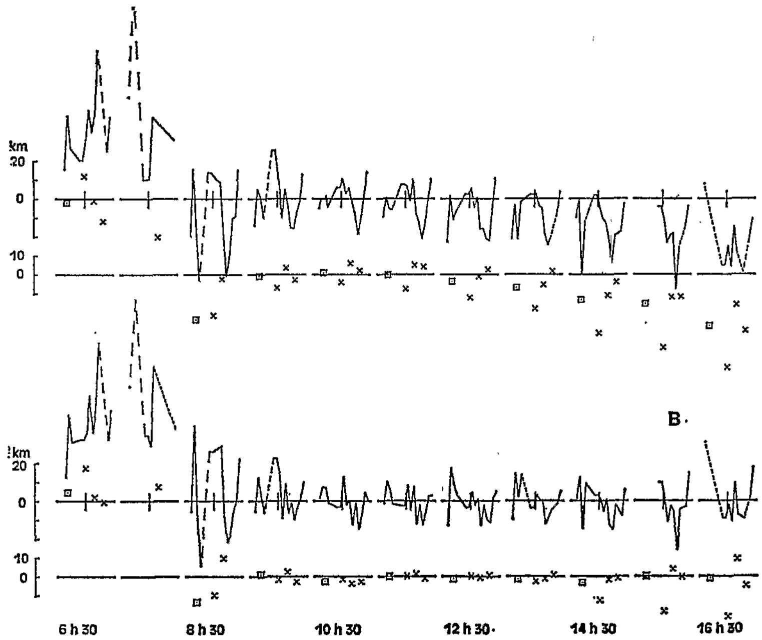

Fig. 2. Locations of the 'apparent' centre (A) or of the 'true' centre (B). Curves: monthly values from November 1968 to March 1970 (missing values, including March and April 1969, are replaced by dashed lines; the vertical line on each monthly graph indicates the middle of the year 1969). Crosses: seasonal D, E and J values. Squares: yearly values. The zero of the graphs is the location of the 'apparent' (or 'true') centre for the yearly value at 1130 LT, i.e. 30·6 km (or 23·6 km) with respect to the parallel 10°N. The 'apparent' centres obtained for the three monthly 0730 profiles which correspond to an electrojet instead of a counter-electrojet are not plotted; they are located close to the average value of 0830. Values of 1730 LT are not drawn because of their too large scatter.

the 'apparent' centres become approximately equal for all the groups; they represent the locations of the 'true' centre c_t (see Table 2). Two other conditions are taken into account: (1) a relative regularity in the variation of α_s with local time, (2) an increase of the Snedecor test value when analysing by the multiple regression. The values α_s thus obtained are drawn in Fig. 1(b), whereas Fig. 2(b) displays, by comparing it with Fig. 2(a), the effects of the three factors β_H, β_Z and α_s. Two main facts appear:

(1) the comparison of the seasonal values at a given hour shows, beyond all question, that the correction by β_H and β_Z is very efficient from 0930 to 1430;

(2) from 0830 to 1630, the effect of α_s is clear with the yearly or seasonal values. We discuss later on the actual action of it.

Table 2. Average locations c (and standard deviation σ), with respect to the parallel 10°N, of the 'apparent' centre for n monthly profiles (c and σ in km). Average locations $c_{H,Z}$ (and their σ's) after reduction by factors β_H and β_Z. Average locations c_t (and their σ's) after final reduction by factor α_s

	1 0830 1030	2 0930 1130	3 1030 1230	4 1130 1330	5 1230 1430	6 1330 1530	7 1430 1630	8 1530 1730
n	42	45	45	44	43	38	34	28
c	26·6	21·0	27·7	25·1	21·6	18·4	13·6	2·6
σ	14·3	10·0	9·8	10·3	11·4	12·2	13·4	34·1
$c_{H,Z}$	14·9	21·0	22·3	22·8	21·9	19·2	13·5	2·9
σ	13·8	8·6	7·6	7·6	8·5	10·1	12·5	35·4
c_t	22·5	22·5	21·8	22·9	23·6	23·7	23·1	22·1
σ	13·9	8·6	7·6	7·6	8·3	8·8	11·0	33·3

Table 3. Electrojet cases. Average locations c, with respect to the parallel 10°N, of the 'apparent' centre for n daily profiles (c in km). Average locations c_H (after correction by β_H) and $c_{H,Z}$ (after correction by β_Z). Average locations c_t of the 'true' centre after correction by α_s

	0630	0730	0830	0930	1030	1130	1230	1330	1430	1530	1630
n	4	50	123	135	165	166	158	147	134	115	101
c	−41·4	−14·9	23·4	29·0	29·5	27·2	24·5	21·7	18·5	17·6	15·5
c_H	−50·8	−19·4	24·5	30·6	31·6	30·9	28·8	24·9	18·5	15·5	14·8
$c_{H,Z}$	−50·9	−19·5	20·2	21·3	20·0	20·8	21·8	21·1	18·0	16·5	14·6
c_t	—	—	28·5	24·6	21·3	20·8	21·3	21·5	21·0	25·3	23·9

Table 3 shows the effect of the successive corrections by the three factors β_H, β_Z and α_s for the 'apparent' centres of the daily profiles. Values are also given for 0630 and 0730 when the electrojet exists at these times. Standard-deviations for c_t vary from 20 km at midday hours to about 40 or 50 km in the early morning or in the late afternoon. The average c_t values vary little, but a very important southward shift seems to be present at 0730 (or 0630); we discuss this apparent anomaly later on.

2.2.2. *The counter-electrojet cases.* With the monthly profiles, the number of counter-electrojet cases (12 at 0630, 7 at 0730, 1 at 0830) is too small for an evaluation of the α_s factor. In the multiple regression analysis, β_Z is the only significant factor, and its effect has an opposite sign with respect to the electrojet cases. In Fig. 2(b), plotted values are corrected by β_Z only. The scatter of the seasonal values for the 2 hr is clearly reduced but the systematic difference with the following hours is always as great.

Table 4. Counter-electrojet cases (as in Table 3; however no correction by β_H is applied to morning values)

	0630	0730	0830	0930	1030	1130	1230	1330	1430	1530	1630
n	108	52	12	1	0	1	1	6	11	14	4
c	63·9	52·1	38·0	91·9	—	89·3	135·6	30·9	39·6	44·3	42·9
c_H	—	—	—	—	—	106·4	128·7	33·6	49·3	52·1	51·4
c_Z	62·3	60·7	62·6	136·4	—						
$c_{H,Z}$						96·4	132·7	31·6	45·7	45·5	41·6
c_t	—	—	—	—	—	96·4	132·2	32·0	49·0	54·3	60·8

Table 4, similar to Table 3, gives the effect of the successive corrections with daily profiles. From 0630 to 0930, factor β_Z only is used with the coefficient $S(\beta_Z)$ determined from the monthly values. Values in the afternoon are arbitrarily corrected by using coefficients $S(\beta_H)$ and $S(\beta_Z)$ coefficients evaluated for the electrojet cases. Standard deviations are high at any hour (40 or 50 km). In the afternoon, the tendency of the centre to be shifted northwards is still present but less clear than in the morning.

3. 'TRUE' CENTRE AND DIP EQUATOR

Table 5, which concerns the electrojet cases, summarizes the effects of the successive corrections for two groups of hours the first of which corresponds to larger amplitudes of the electrojet and, consequently, to a better determination of the 'apparent' centre. One may estimate that the 'true' centre is at about 23 km North of the parallel 10°N at midday hours. With the action of factor α_s, one obtains a nearly identical value from 0830 to 1630. By taking factor α_i into account, the final location of the 'true' centre would be 25 km.

The dip equator is 33·6 km North of the parallel 10°N on the meridian 17°E. But, according to Table 1, the observed 'true' centre falls between the 'efficient' dip equators corresponding to $\Delta\Lambda = 30° - 5°$E and $35° - 0°$E. Our conclusion will be that the longitude sector width within which the electrojet phenomenon smooths the sinuosities of the dip equator is approximately 2 hr in longitude in Central Africa.

In the case of the morning counter-electrojet, standard-deviations of the 'true' centre are respectively 6·7, 21·3 and 44·7 km for the seasonal, monthly and daily profiles. The average position, at 70 km North of the parallel 10°N, corresponds to a northward shift of 45 km with respect to the normal electrojet. Such a shift is partly due (about 15 km) to the analysis method (see Paper I, Section 4.4.1) which introduces systematic errors when the amplitude of the $S_R{}^E(H)$ is small. However, on a day as 6 June 1969, the $S_R{}^E(H)$ reaches −60 gammas at

Table 5. Electrojet cases. Average values c (and standard deviations), for various classes of n profiles, of the 'apparent' centre. Average values c_H (after correction by β_H), $c_{H,Z}$ (after correction by β_Z) and c_t (after correction by α_s)

	yearly	seasonal	monthly	daily
		0930–1330		
n	5	15	74	791
c	28·6 ± 2·9	28·5 ± 6·7	26·8 ± 10·5	26·5 ± 18·1
c_H	30·3 ± 2·9	30·5 ± 3·2	31·6 ± 10·3	29·4 ± 24·8
$c_{H,Z}$	21·9 ± 1·3	22·0 ± 2·3	22·9 ± 8·1	21·0 ± 20·8
c_t	22·8 ± 1·2	22·9 ± 1·7	23·2 ± 8·1	21·9 ± 20·9
		0830–1630		
n	9	26	119	1264
c	20·6 ± 10·0	20·7 ± 14·0	22·2 ± 13·8	23·7 ± 24·1
c_H	21·8 ± 10·4	21·9 ± 13·0	25·3 ± 15·2	25·3 ± 29·6
$c_{H,Z}$	16·4 ± 7·8	16·7 ± 10·1	19·1 ± 11·8	19·7 ± 26·1
c_t	21·3 ± 4·1	21·5 ± 6·8	23·2 ± 10·7	23·7 ± 26·3

the profile centre, and the centre is still located at +70 km. Consequently, the 'true' centre of the morning counter-electrojet does not coincide with the 'efficient' dip equator as does the normal electrojet.

For the 37 afternoon daily profiles where a counter-electrojet occurs, the location of the 'true' centre is 53·0 ± 46·8 km. Corrections by various factors are much less valid, but a discrepancy with the normal electrojet is certainly present as with the morning counter-electrojet.

4. DISCUSSION

4.1. *Actual action, and physical meaning, of various factors α and β*

The evaluation made, with the Richmond model, of the importance of factor α_i is probably correct, and its meaning is obvious (stronger currents where the total force of the main magnetic field is smaller). However too many other factors prevent one from asserting that it actually exists. From an experimental point of view, no proof is brought in this work of its existence. In particular, the concept of dip equator, in the region of our observations, is too hazy for demonstrating the existence of a 2 km shift due to a given factor having a constant effect.

The actual action of the effects of factors β_H and β_Z is unquestionable according to the decrease of the standard-deviations which they involve (see Table 5). The physical meaning of β_H is obvious. When the $S_R{}^P(H)$ is larger on one side of the 'true' centre, the electrojet currents are denser on the same side. Then, through the analysis made with a symmetrical model, one obtains an 'apparent' centre which is shifted towards this side. As an average, the $S_R{}^P(H)$ is larger at the South than at the North. Consequently, the 'apparent' centre (see first line of Table 5) is more South than the centre corrected by factor β_H (see second line of Table 5). According to the value of $S(\beta_H)$ (i.e. 6·9 km/gamma), the shift can exceed 10 km since the β_H asymmetry is sometimes of ±2 gammas.

The physical effect of β_Z (the value of $S(\beta_Z)$ is −1·3 km/gamma) is more difficult to grasp because this factor has a twofold meaning: it contains information about both the curvature of the $S_R{}^P$ current lines ($\beta_Z = 0$ would mean that one is at the border between the planetary vortices), and the latitudinal gradient (as does β_H) of the current lines. According to average values of β_Z, the electrojet would be, as an average, under the influence of the northern planetary vortex ($\beta_Z < 0$) if the accent is put on the curvature information (β_D values confirm that point). Now, the effect of the β_Z correction, as an average, is a southward shift (compare second and third lines of Table 5). It would mean that the currents of the electrojet, when it is embedded within the northern vortex, are more intense at the north of the centre than at the south. An asymmetry liable to cause such an effect would be as follows: the curvature of the primary electric field is then directed towards the exterior of the curvature of the lines of force at the north of the dip equator, and towards the interior at the south. Furthermore factors β_H and β_Z, as an average, act in the opposite sense, and the β_Z effect is greater (compare first, second and third lines of Table 5).

The actual action of the effect of factor α_s is not at all proved by the decrease of the standard-deviations. Indeed α_s values have been chosen in order to obtain such a decrease. The only proof of its reality would be an analysis of observations made, from a sufficient number of stations, on a meridian where the 'shape' of the dip equator, on either side, would be clearly different. Then, if the daily variation of the 'apparent' centre differs from that obtained on the meridian 17°E (see Fig. 2a) and is similar to the shape of the dip equator in this region, the proof of the influence of factor α_s would be definite. At present, a comparison of variation α_s in function of the local time with the shape of the dip equator (see Fig. 1) only suggests that such an effect is possible. Note that the systematic error in the centre determination (see Paper I, Section 4.4.1) when the $S_R^E(H)$ is very weak is not the cause of the afternoon southward shift of the afternoon southward shift of the 'apparent' centre (see Fig. 2a) since the sense of the error is in the opposite direction.

4.2. *Stability of the 'true' centre*

ONWUMECHILLI (1967) summarized previous results concerning the location of the electrojet centre. A comparison with our own results is difficult because none of the previous profiles, including that of FORBUSH and CASAVERDE (1961), comprises a latitudinal extent great enough to determine accurately the centre location.

The 1·7 km standard-deviation for the 'true' centre of the 0930–1330 *seasonal* profiles (see Table 5) is very small when compared to the spread of the nine recording points over 3000 km. The standard-deviation decrease between the 'apparent' centre (6·7 km) and the 'true' centre (1·7 km) is extremely significant. It means that the 'apparent' variations of the centre can be fully reduced by taking the S_R^P variability into account (at these hours, factor α_s varies little). And such an effect acts in two ways: either from one season to another at a given hour, or from one hour to another at a given season (compare Fig. 2a, b). When one considers all the hours (0830–1630), a relative unstability appears but one can firmly state that it is due either to the uncertainty of the determination of coefficients $S(\beta_H)$ and $S(\beta_Z)$—we assume that the effect of the factors is linear—or to an inaccurate evaluation of factor α_s.

Standard deviations are much higher with monthly or daily profiles (see Table 5) although the average value for the 'true' centre is very similar. Are such deviations true? At midday hours, some of these deviations obtained from the daily profiles come from cases where the electrojet intensity is small. We suspect that others have to be attributed to the deficiency of the analysis method (see Paper I, Section 4.2.2) with regard to the definition of the $S_R^P(Z)$; when looking at daily profiles corresponding to large deviations of the centre, one can observe that the $S_R^P(Z)$ appears poorly determined in relation to the $S_R(Z)$. In other words, it is probable that the stability of the centre is greater than one may think from the monthly or daily standard deviations of Table 5.

4.3. *Coincidence, and deviation, between the 'true' centre and the dip equator*

With regard to the electrojet 'true' centre, the standard deviation ($\pm 1·7$ km) obtained at midday hours for the seasonal values is ten times smaller than the shift of the dip equator over 2° of longitude on either side of the meridian 17°E. It is the reason for which we believe that the concept of 'efficient' dip equator is much more suitable, for Central Africa, than the concept of 'local' dip equator. When choosing a longitude sector of 2 hr width, (between $\Delta\Lambda = 30° - 5°$ and $\Delta\Lambda = 35° - 0°$, see Table 1) for the 'efficient' dip equator, the coincidence with the electrojet 'true' centre ($+25$ km) appears remarkable. At other hours, it is still questionable whether large shifts of the dip equator (factor α_s) on either side of the meridian of observation have an influence on the location of the electrojet centre or not.

With regard to the morning counter-electrojet centre, a northward shift of about 40–50 km with respect to the dip equator seems an experimental fact well established for Central Africa. In the afternoon, such a shift is much less systematical but remains clear in some cases. We would like to suggest an explanation of this different behaviour of the counter-electrojet.

The occurrence of the counter-electrojet needs the existence of a primary westward electric field at equatorial latitudes. At present, no known phenomenon can bring about a primary electric field in the equatorial latitudes themselves. Then one is forced to assume that the primary westward electric field has a planetary source as the eastward electric field (see GOUIN and MAYAUD, 1969, who attempt to establish a link between counter-electrojet events and variability of the S_R at mid-latitudes). In these conditions, a possible explanation of the northward shift of the counter-electrojet is to assume that the component of the S_R field which feeds the counter-electrojet originates mainly (or only?) in the northern hemisphere. Such an asymmetry would be the reason for the average shift; day-to-day variability of the importance of the asymmetry could bring about more or less important movements of the 'apparent' centre. One knows (Gouin and Mayaud, 1967) that the morning counter-electrojet amplitude varies greatly with longitude (it is the largest in African longitudes). One also knows (see, for instance, Gouin and Mayaud, 1967, Hutton, 1970; Onwumechilli and Akasofu, 1972; Kane, 1973; Rastogi, 1973; Schieldge, 1974) that the afternoon counter-electrojet 'events' are sometimes very fugacious from one longitude to another. These two facts are the sign of large longitudinal variations in the planetary source. Then it is also quite plausible that this planetary source of the counter-electrojet varies greatly from one hemisphere to another, and it would do so in the morning more systematically than in the afternoon.

The abnormal fact of a southward shift of the 'apparent' centre of the normal electrojet itself, at 0630 and 0730 (see Table 3), would be a possible confirmation of this assumption. On the one hand, 42 (out of 50) of 0730 cases occur during the December solstice. On the other hand, when one looks at the D-component profiles, one finds out that, for many of them, the $S_R(D)$ is negative (i.e. westwards); it indicates that, at this time of the day, the electrojet region is under the influence of the southern vortex. We made, for these 50 cases, a new attempt with factor β_D; it failed because of the too large dispersion of the values. But when one classifies the 50 cases in two groups with respect to the $S_R(D)$ value (for instance, $\beta_D < -5$ gammas—26 cases, and > -5 gammas —24 cases), the average 'apparent' centre locations are $-28{\cdot}1$ km and $-0{\cdot}3$ km respectively. Therefore the 'apparent' centre is more south when the influence of the southern vortex is larger according to the $S_R(D)$ value.

But if such an assumption is valid in the early morning, what about the late afternoon? Is the southward shift (see Fig. 2a) caused by a similar phenomenon? The fact is that, according to the value of $S_R(D)$, equatorial regions are, at that time of the day, more often under the preponderant influence of the northern vortex, and the above assumption would then mean a northward shift. Consequently, it seems that the factor α_s is probably valid for explaining the southward shift in the late afternoon. Furthermore, this factor could be underestimated if a northward shift (due to the predominant northern vortex) is superimposed. Besides the more south location of the 'apparent' centre at December solstice (see Fig. 2b, 1530 and 1630), a time where the northern vortex is less predominant, tends to confirm such a superimposition of both effects.

Finally, erratic deviations between the dip equator and the centre of either the counter-electrojet or the electrojet become quite important in the morning and afternoon periods. A reasonable explanation would be the large gradient which exist at those times in the planetary vortices. Indeed, in the early morning (or in the late afternoon), the $S_R{}^P$ asymmetries have effects probably very different from those of the asymmetries at midday hours. With the latter, both the planetary vortices are present in equatorial (or low latitudes) regions, and the latitudinal gradient of the primary electric field is never very large. But, in the early morning or in the late afternoon, one vortex can entirely predominate and, as shown by many planetary analyses (see, for instance, Price and Wilkins, 1963), large gradients take place. These could account for day-to-day large deviations of the 'apparent' centre at these times of the day.

Acknowledgements—The authors thank the Directors of Binza and Tamanrasset observatories for providing their magnetograms. Other data used in this study have been acquired with the support of "Recherche Coopérative sur Programme" (RCP 168) of the C.N.R.S. We are greatly indebted to M. Villeneuve, Chief of the ORSTOM Mission at Sahr (Chad), for the wonderful quality of the records in the temporary stations.

REFERENCES

Bennet C. A. and Franklin K. L. 1954 *Statistical Analysis in Chemistry and the Chemical Industry*. John Wiley, New York.
Fambitakoye O. and Mayaud P. N. 1975 *J. atmos. terr. Phys.* **38**, 1.
Gouin P. and Mayaud P. N. 1967 *Annls Géophys.* **23**, 41.
Gouin P. and Mayaud P. N. 1969 *C. R. Acad. Sci., Paris*, **268**, 357.
Hutton R. 1970 *Annls Géophys.* **26**, 921.
Onwumechilli A. snd Akasofu S. I. 1972 *J. Geomagn. Geoelect.* **24**, 161.
Price A. T. and Wilkins G. A. 1963 *Phil. Trans. R. Soc. London.* **A256**, 31.
Rastogi R. G. 1973 *Planet. Space Sci.* **21**, 8, 1355.
Richmond A. D. 1973 *J. atmos. terr. Phys.* **35**, 1083.

Reference is also made to the following unpublished material.

Forbush S. E. and Casaverde M. 1961 Carnegie Inst. Wash., Publ. 620.
Schieldge J. B. 1974 Ph.D. Thesis, Univ. of California, Los Angeles
Kane J. C. 1973 Rept. AER-73-08, Phy. Res. Lab., Amhedabad, India.

Journal of Atmospheric and Terrestrial Physics, Vol. 38, pp. 113 to 121. Pergamon Press, 1976. Printed in Northern Ireland

Equatorial electrojet and regular daily variation S_R—III. Comparison of observations with a physical model

O. FAMBITAKOYE
S.S.C.-ORSTOM 93, Bondy, France

P. N. MAYAUD*
Institut de Physique du Globe, Université Paris VI, France

and

A. D. RICHMOND†
Laboratoire de Physique de l'Exosphère, Université Paris VI, 75230 Paris, France

(*Received* 10 *March* 1975)

Abstract—Latitudinal profiles of magnetic variations across the magnetic equator in Chad, are compared with a physical model of the equatorial electrojet which includes the effects of ionospheric winds and plasma instabilities. According to the model, east–west winds can have two types of influence on the ionospheric currents, both of which are clearly reflected in the observed magnetic profiles. Firstly, the winds can create the appearance of a secondary current ribbon, opposed to and wider than the primary electrojet ribbon due to an east–west electric field. Secondly, winds can augment (or diminish) the level of the 'planetary' current component in the low-latitude region, in comparison to that due to a pure electric field. We present arguments strongly supporting the existence of mean westward winds at high altitudes (125–200 km) in the daytime equatorial ionosphere. The data also suggest the possible presence of plasma instability effects, which the model indicates should tend to inhibit the electrojet enhancement current and widen the primary current ribbon. The influence of the two-stream (Type I) instability, which the model takes into account, is not entirely obvious. However, we suggest that the gradient-drift (Type II) instability, which the model does not take into account, may have an important influence on the electrojet currents.

1. INTRODUCTION

Previous articles of this series (FAMBITAKOYE and MAYAUD, 1975a, hereafter called Paper I; and FAMBITAKOYE and MAYAUD, 1975b) have described features of the ground-level magnetic field created by the equatorial electrojet and measured at a chain of nine stations in Africa. The present article compares these observations with a physical model of the electrojet (RICHMOND, 1973a) in order to examine some features of the equatorial ionosphere. We are particularly interested in examining the effects of ionospheric winds and plasma instabilities on the magnetic profiles, two features which are incorporated into Richmond's model.

STENING (1969) pointed out that winds in the F-region could produce a secondary maximum, at around 7°–10° magnetic latitude, in the latitudinal profile of the magnetic H (horizontal) perturbation, as sometimes seems to occur in South America (HUTTON, 1967). RICHMOND (1973a) considered theoretically the effects of winds on equatorial ionospheric currents, and found in particular that (a) an east–west wind must vary in altitude in order to produce any current, and (b) for east–west winds whose altitude variations are not extreme, very little current is produced within about 2° of the magnetic equator, but substantial current can be produced at higher latitudes. RICHMOND (1973b) also demonstrated that oscillatory features observed in the height profiles of ionospheric currents measured by rockets a few degrees off the magnetic equator (MAYNARD, 1967) can be explained by winds with a vertical structure characteristic of the (1, 1) tidal mode. In the present paper we examine in more detail the influence of east–west winds on the height-integrated current density and on the magnetic profiles in the equatorial region.

RICHMOND's (1973a) model also includes the effects of the two-stream (Type I) instability, which tends to limit the electrojet current density

* Contribution I.P.G. No. 134.
† Present address: High Altitude Observatory, P.O. Box 3000, Boulder, Colorado 80303, U.S.A.

when the polarization electric field exceeds a threshold (ROGISTER, 1971; SATO, 1972). It does not, however, include the effects of the more common gradient-drift (Type II) instability, which may also tend to reduce the polarization electric field and electrojet currents (SATO, 1974), but which is more difficult to quantify. RICHMOND's (1973b) examination of available data was inconclusive as to whether the two-stream instability indeed affects electrojet currents as predicted; our comparison of magnetic profiles with his model is similarly inconclusive. We shall suggest, however, that the gradient-drift instability may have an important influence on electrojet currents.

2. WIND EFFECTS

The eastward current density, J_ϕ, due to an eastward component of the neutral air wind, v_ϕ, is determined in RICHMOND's (1973a) $\sigma_0 = \infty$ model by

$$J_\phi = \sigma_2 B_0 v_\phi - \sigma_2 B_0 \left[\int_{s_1}^{s_2} \sigma_1 v_\phi \, ds\right] \Big/ \left[\int_{s_1}^{s_2} \sigma_1 \, ds\right] \quad (1)$$

where σ_1, σ_2 are the Pedersen and Hall conductivities, B_0 is the geomagnetic field strength, and where the line integrals are taken along the line of force passing through the point in question, through the entire conducting region of the ionosphere. The first term on the right-hand-side of (1) represents the Hall current driven by the dynamo electric field $\mathbf{v} \times \mathbf{B}$, while the second term represents the eastward Hall current driven by an electrostatic field, which is generated by the wind. Notice that

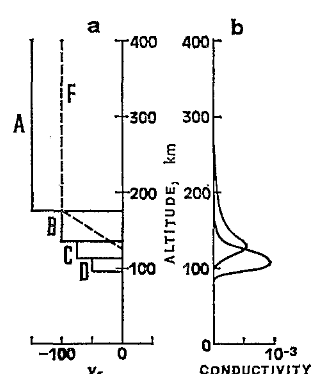

Fig. 1. (a) Height profiles of westward winds used to calculate currents in Figs. 2 and 3. (b) Height profiles of ionospheric conductivities. The parameters used in RICHMOND's (1973a) model are $B_0 = 3{\cdot}2 \times 10^{-5}$ T, $f = 1{\cdot}0$, $F_{10{\cdot}7} = 140 \times 10^{-22}$ W m^{-2} Hz^{-1}, $\chi = 0°$.

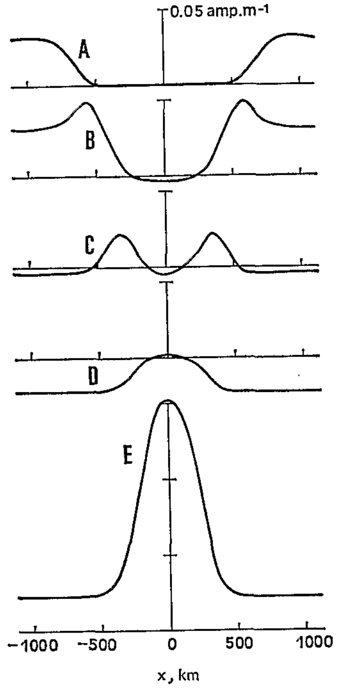

Fig. 2. Latitude profiles of height-integrated ionospheric currents calculated using wind profiles A–D of Fig. 1(a), and using an eastward electric field of $0{\cdot}4$ mV m^{-1} (profile E).

the first term gives a current in the same sense as the wind, whereas the second term gives a current in the opposite sense of the mean wind along the line of force, weighted by σ_1. Under certain circumstances the two terms can tend to cancel each other, such for a constant wind or, at the magnetic equator below 125 km, for a wind whose spatial variations are not too rapid (see, RICHMOND, 1973a, for a fuller discussion of this effect). To illustrate the effects of winds at different altitudes, we have calculated the height-integrated eastward current density, I, for four profiles of westward winds (v_ϕ negative) illustrated in Fig. 1(a). For reference, the height profiles of σ_1 and σ_2 are shown in Fig. 1(b). Each of the four wind profiles is constant over a certain height range and zero outside this range: profile A is 150 ms^{-1} above 175 km; profile B is 100 ms^{-1} between 135 and 175 km; profile C is 75 ms^{-1} between 113 and 135 km; and profile D is 50 ms^{-1} between 95 and 113 km. The resultant currents are shown in Fig. 2 as a function of distance x from the magnetic equator. Profile E, at the bottom of Fig. 2, is the height-integrated current density due to an eastward electric field of $0{\cdot}4$ mV m^{-1}, without any wind effects.

For profiles A and B, the currents represent mainly the effects of an electric field which is generated in regions where $\sigma_1 v_\phi$ is large, and which is transferred down magnetic lines of force to the E-region to drive the eastward Hall currents. The deficit of currents around the equator is due to the fact that magnetic field lines which penetrate the E-region close to the equator do not reach up into the region where the winds exist, so that no electric field is generated along these field lines. For profile D, the currents represent mainly the direct effects of the $\mathbf{v} \times \mathbf{B}$ dynamo electric field, rather than of an electrostatic field. The deficit of currents around the equator in this case is due to the creation of an electrostatic field on magnetic field lines which peak in the E-region; this electrostatic field tends to cancel the dynamo $\mathbf{v} \times \mathbf{B}$ electric field on these field lines. The profile C represents an interesting case where the height-integrated currents due to the dynamo $\mathbf{v} \times \mathbf{B}$ electric field and due to the electrostatic field nearly cancel both near the equator and several degrees from the equator, but not in the intermediate regions 200–500 km on either side of the equator. It should be noted that the current profiles A–E would be inverted if the signs of v_ϕ or E_ϕ were reversed.

One can imagine how different combinations of wind profiles and E_ϕ values can produce more or less complicated latitudinal profiles of current density. As one quite plausible example we combine the current profiles E and F of Fig. 3(a), which are produced respectively by an eastward electric field of 0·4 mV m^{-1}, and by the high-altitude westward wind profile F shown by a dashed line in Fig. 1(a). The combined current profile is shown by the solid line in Fig. 3(b). The analysis of Paper I would resolve this current profile into three components: a smooth $S_R{}^P$ component, a main eastward current ribbon of about 350 km half-width, and a secondary westward current ribbon of about 700 km half-width. The dashed curve 1 in Fig. 3(b) shows the $S_R{}^P$ current alone. The dashed curve 2 shows the sum of the $S_R{}^P$ component and the westward current ribbon. The solid curve 3 is the sum of all three components. (In practice, the sum of these three components would not coincide exactly with the sum of profiles E and F, because only a finite number of adjustable parameters is used to resolve the three components.) From this example, it is apparent that the size of the $S_R{}^P$ component is strongly dependent on the strengths of both the electric field and the wind. On the other hand, the strength of the main current ribbon is largely, but not wholly, dependent on the electric field strength, while the strength of the secondary current ribbon is largely, but not wholly, dependent on the strength of the wind. It is important to note that none of the three deduced current components represents by itself an isolated physical phenomenon.

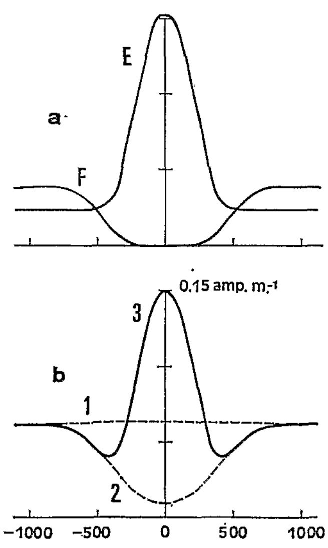

Fig. 3. (a) Latitude profiles of height-integrated ionospheric currents using $E_\phi = 0{\cdot}4$ mV m^{-1} (profile E) and wind profile F of Fig. 1(a). (b) Combination of current profiles E and F (solid line). See text for explanation of dashed lines.

Figure 4 gives an example of observed hourly profiles of the $S_R(H)$ and $S_R(Z)$ magnetic variations on a quiet day when, at certain hours, the effects of winds are particularly striking. At 0830 and 0930, the H and Z profiles are more or less what one would expect to obtain from an electrojet driven by a pure eastward electric field without winds, i.e. from a current such as that of profile E in Fig. 2, with the amplitude appropriately adjusted. The growth of the current intensity between 0830 and 0930 is partly due to increased ionospheric conductivity, but probably more importantly to an increased E_ϕ. Beginning at 1030, two qualitative changes occur in the H profiles: the $S_R{}^P$ is larger, with respect to the value of S_R at the equator, than at 0930, and the S_R curves dip below the $S_R{}^P$ curves on either side of the electrojet. Both of these changes can be explained by the presence of a westward wind at high altitudes, which would produce a current profile like that of Fig. 3(b). It appears that the currents due to E_ϕ decrease between 1030 and 1530, whereas those due to the winds maximize roughly around 1300.

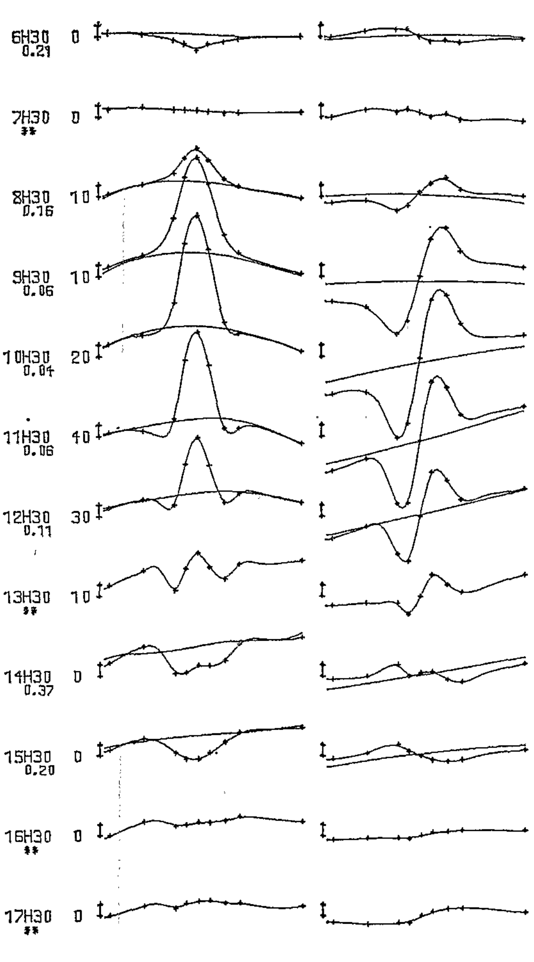

Fig. 4. Hourly latitudinal profiles of $S_R(H)$ (left) and $S_R(Z)$ (right) in Chad on 29 January 1969. At the left is given 15° E time; below each time is a number giving the relative size of the residues for the analysis of the profiles, provided this number is not greater than 0·40 (see FAMBITAKOYE and MAYAUD, 1975a, for further explanation). The vertical bars to the left of each profile represent 10 γ; for the Z profiles the horizontal mark at the bar represents the base level, while for the H profiles this mark represents a value either 0 γ, 10 γ, 20 γ, . . . , above the base level, as indicated to the left. The crosses (+) indicate observed values, adjusted to 15°E time. When the relative residues are less than 0·40, the smooth $S_R{}^P$ curves are also drawn. At the bottom are given the date, the a_m values for 0700–1000, 1000–1300, 1300–1600, 1600–1900 15°E time, and the average a_m value for the 24 hr day.

At 1530, the magnetic effects appear to be those of a single westward ribbon of current, superimposed on eastward $S_R{}^P$ currents. This profile could be simulated by a high altitude westward wind (such as that of profile F) plus a small westward electric field, to account for the fact that $S_R(H)$ actually becomes negative at the equator. The net result is an apparent 'counter-electrojet' which is wider than the eastward electrojet of 0830.

The reader will notice that we have emphasized high altitude (i.e., above 125 km) winds rather than low altitude winds, even though it would be possible to explain the same effects in terms of low altitude winds. (The currents produced by a constant westward wind above, say, 125 km are identical to those produced by a constant eastward wind of the same magnitude below 125 km.) Our preference for high-altitude winds is based on observations of midlatitude thermospheric winds (e.g., KOCHANSKI, 1964; ROSENBERG, 1968; BEDINGER, 1972) which reveal that below 125 km the winds vary strongly with altitude, but that above 125 km height variations are much less pronounced. Since the height-integrated current density depends on a type of height integral of the wind velocity over a certain altitude range, the contribution by low-altitude winds will in general be considerably less than that by high-altitude winds, if the as yet unmeasured thermospheric winds in the equatorial regions are qualitatively similar to those at midlatitudes.

From the variability of H and Z profiles which have been observed in Chad (see FAMBITAKOYE, 1974), and from the variability of various derived parameters shown in Paper I (Fig. 11 and Table 5), we conclude that the thermospheric winds are variable not only during the course of a day but also from day to day and month to month. Nevertheless, there seem to be average winds present throughout the year, which make their presence known by their characteristic effects on the H and Z profiles averaged for the year (see Fig. 1 of Paper I). In particular, secondary ribbons are present in the yearly profiles between 1130 and 1530 local time, suggestive of high-altitude westward winds during this part of the day. The electric polarization field which such a wind would generate is also in the right sense to explain WOODMAN's (1972) observations of westward plasma drifts in the daytime F-region.

3. CURRENT INTENSITIES AND ELECTROJET WIDTH

With an understanding of how the equatorial currents can be influenced by neutral-air winds, we are now prepared to make quantitative comparisons of some electrojet parameters derived from the observations with predictions of the physical model. The two quantities of interest to us are the width of the electrojet and the relation between the current of the electrojet and the current associated with the $S_R{}^P$ variations. When speaking of the width of the observed electrojet we mean the value a in the law of current distribution

$$I(x) = I_0[1 - (x - c)^2/a^2]^2, \quad |x - c| < a \quad (2)$$

for the primary current ribbon, as derived from the observations by the analysis described in Paper I. For the model we mean the value of a determined by least-squares fitting this law of current distribution to values of the height-integrated "electrojet enhancement current density" of RICHMOND (1973a). When speaking of the current associated with the $S_R{}^P$ variations, we mean the value I_P defined by

$$I_P = 0{\cdot}72 S_R{}^P(H)/(0{\cdot}2\pi) \quad (3)$$

(see Paper I), where the value of $S_R{}^P(H)$ is in gammas, measured at $x = c$, and the value of I_P is in A/m. The factor 0·72 is assumed to be that portion of $S_R{}^P(H)$ attributable to external currents only. For the model, we assume that I_P corresponds to the height-integrated "background current density" of RICHMOND (1973a). The third parameter with which we are concerned is the total height-integrated current density at the centre of the electrojet, I_T, defined for the observations as

$$I_T = I_P + I_{0,1} + I_{0,2}$$

where $I_{0,1}$ and $I_{0,2}$ are the derived values of I_0 for the main and secondary current ribbons.

According to the model, the current I_T is nearly independent of any winds which may be present, but it is strongly dependent on the eastward electric field, E_ϕ. In the absence of current-limiting effects of the two-stream plasma instability, I_T and E_ϕ are linearly related. When E_ϕ passes a threshold value, the two-stream instability comes into play and reduces the value of I_T, so that for very large values of E_ϕ, I_T approaches saturation. Although the functional relation between E_ϕ and I_T is not always linear, it is always monotonic, so that according to the model, I_T should be a good parameter with which to represent E_ϕ.

In Figs. 5 and 6 are plotted derived values of I_P and a, respectively, as functions of I_T. Included are all hourly values between 1030 and 1330, inclusive, for 126 quiet days for which the analysis did not fail, with the additional restriction that the corresponding a_m index for any hour plotted not be greater than 12. Positive values of I_T indicate a normal (eastward) electrojet; negative values indicate a (westward) counterelectrojet. The lack of points for $10 < I_T < 60$ mA m^{-1} is due primarily to the fact that the analysis fails when I_T is approximately equal to I_P, i.e. when $I_{0,1}$ and $I_{0,2}$ are small. The asterisks (*) give the averages of the points for intervals of 20 mA m^{-1} in I_T. The continuous lines in Figs. 5 and 6 are derived from the model with a variable E_ϕ but without any winds, using parameters appropriate to the longitude sector and solar activity level of the observational period. The solar zenith angle used is 20°, approximately the mean for the observations. Variations in the solar 10·7 cm flux or in the zenith angle would probably cause not much more than 10% differences each in the theoretical line in Fig. 5, and only slight differences in the theoretical line in Fig. 6; in any case these variations would be much less than the dispersion of the points.

For $I_T > 240$ mA m^{-1}, the theoretical values in Figs. 5 and 6 deviate from straight lines because of the influence of the two-stream instability. The upward bending of the curve in Fig. 5 results from the fact that I_P is linear with E_ϕ, but that I_T approaches saturation as E_ϕ increases. The increased values of a which the curve in Fig. 6 shows for $I_T > 240$ mA m^{-1} are due to the fact that the instability changes the shape of the latitudinal current profile, flattening somewhat the electrojet peak at the equator. Unfortunately, the observations contain an insufficient number of points for $I_T > 240$ mA m^{-1} to permit a valid test of the two-stream instability effects predicted by the model. This deficiency might not occur in a period of very high solar activity like the IGY, when currents are generally much stronger than those of our observational period.

In both Figs. 5 and 6, two features are noteworthy: a large dispersion of points, and a displacement of the average observed values above the theoretical lines. To explain the dispersion, a number of factors are possible, of which the three most important are probably (1) errors in the determination of the ionospheric current distribution from the observed magnetic variations (2) variable upper atmospheric parameters (temperature, composition, longitudinal variations of the electric fields etc.) which are not taken into account in the model, and (3) variable ionospheric winds. The first two factors would also be responsible for the considerable dispersion which RICHMOND

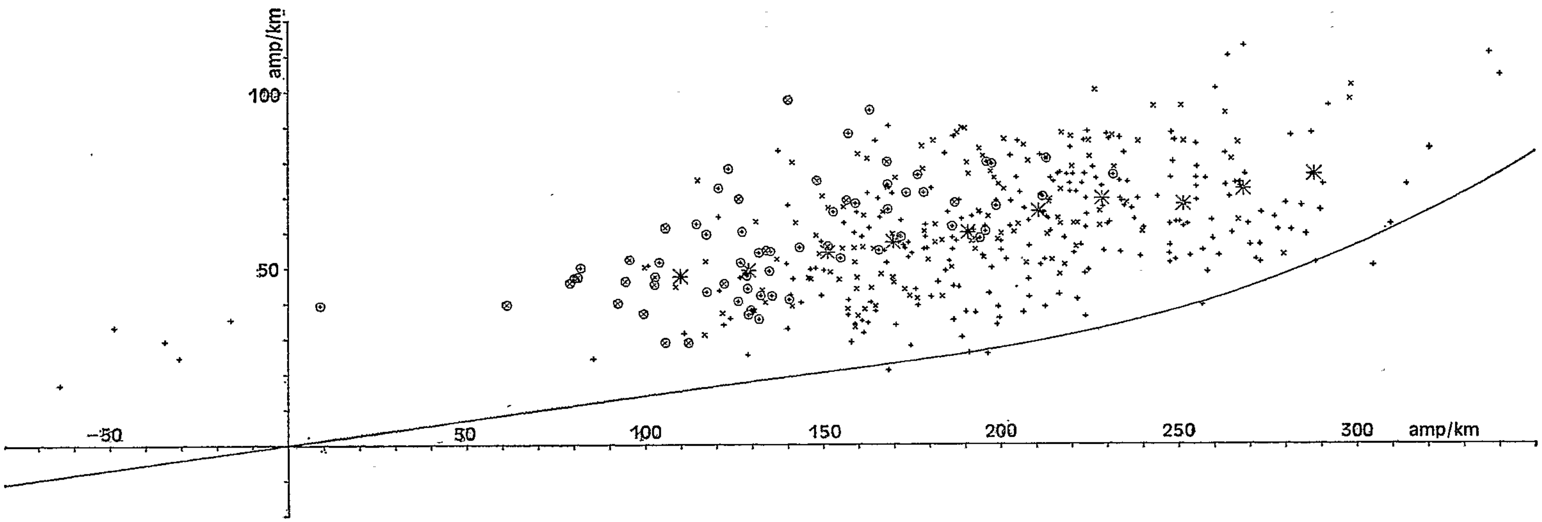

Fig. 5. Derived (points) and theoretical (line) values of I_P vs I_T (see text). A "+" represents a value when a single current ribbon was detected; a "×" represents a value when two oppositely directed ribbons were detected. A circled point indicates that the relative residues (see FAMBITAKOYE and MAYAUD, 1975a) were between 0·20 and 0·40, so that the point is less reliable than an uncircled point.

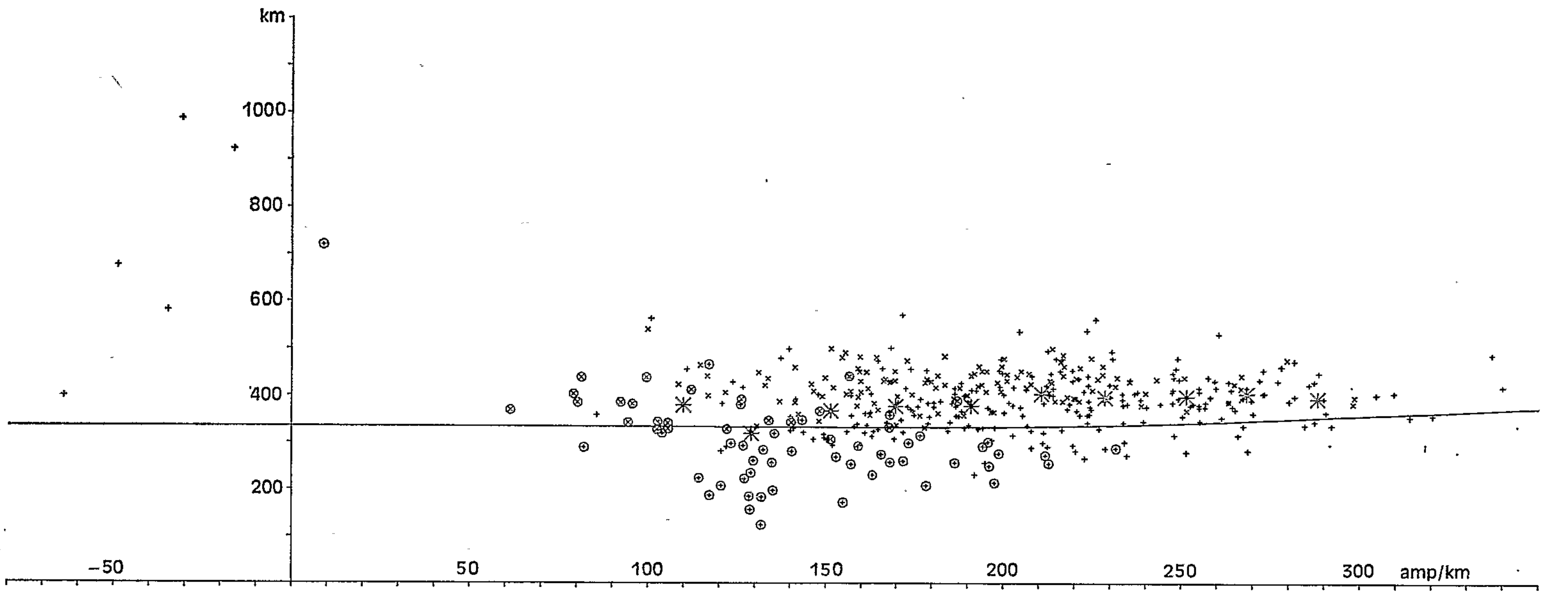

Fig. 6. Derived (points) and theoretical (line) electrojet widths (see text and caption to Fig. 5).

(1973b) found in his Fig. 8, comparing H at Huancayo with E_ϕ in the F-region above Jicamarca. We can also surmise that variable winds are an important factor in causing dispersion, based on the observed variability of H and Z profile shapes (Fambitakoye, 1974) which we have already discussed as being influenced by winds.

To explain the consistent displacement of the observed values of I_P above the theoretical line in Fig. 5, we examine three possibilities. (1) The observed enhancement of I_P may be caused by winds. This explanation is consistent with the previously discussed presence of secondary ribbons in the yearly profiles for the hours of the day used in this figure. Since the enhancement of I_P does not appear to be strongly dependent on I_T, the winds would not seem to be strongly correlated with I_T (or E_ϕ). (2) Non-ionospheric currents, such as those at the magnetopause, could augment the midday H variation at low latitudes and hence augment the derived values of both I_P and I_T equally. These augmentations would shift the points above the theoretical curve, as observed. However, it would require a midday magnetospheric source on the order of 40 γ to account for the observed shift, which is considerably more than models of magnetospheric sources yield (Olson, 1970). This explanation is all the more doubtful when it is noted that predicted nighttime magnetic variations by Olson's (1970) model are practically undetectable on our magnetograms. (3) For the positive values of I_T, the increased I_P/I_T ratios over theoretical values may be partly due to an underestimation of instability effects in the model. If, for example, the neglected gradient-drift instability acted to reduce electrojet currents (I_T) from the model values, the theoretical values of I_P/I_T should be increased.

To explain the fact that the mean derived electrojet widths are greater than the theoretical values in Fig. 6, we again examine three possibilities. (1) Winds, by distorting the theoretical H and Z profiles from their wind-free shapes, could often result in increased derived widths. For example, a wind which had the effect of adding a second, wider current ribbon in the *same* sense as the main electrojet ribbon, would result in only a single ribbon being detected, wider than the main ribbon itself, because the analysis is incapable of distinguishing two current ribbons in the same sense. This effect is most likely responsible for the large widths derived when I_T is negative and small, for which wind effects are probably relatively important. Nevertheless, even when we examine only the cases where two oppositely directed ribbons were detected (×), the discrepancy between theoretical and mean derived widths remains. (2) Gross errors in the assumed ionospheric parameters used in calculating conductivities in Richmond's (1973a) model could cause an underestimation of model electrojet widths. Such errors, if they exist, could also explain the fact that the model seems to underestimate the height of the electrojet by some 5 km (Richmond, 1973b). Increasing the height of the electrojet at the equator would also increase the width, as a greater length of the magnetic field lines with strong polarization electric field would then be contained in the conducting region of the ionosphere. (3) The neglect of any gradient-drift instability effects could cause an underestimation of instability-produced electrojet widening. The gradient-drift instability could be even more effective than the two-stream instability in widening the electrojet, since the former occurs primarily in the lower levels of the electrojet, where the electron density gradient is strongest, and hence could raise the effective height of the electrojet currents, leading to the electrojet-widening effect mentioned above.

It is important to recognize that any physical mechanism invoked to explain why the electrojet is wider than the model predicts, will probably also influence the theoretical relation between I_P and I_T, so that it is necessary to consider the two phenomena together. Our own impression is that winds are an important cause of the discrepancies between theory and observation displayed in Figs. 5 and 6, and that a possible underestimation of instability effects due to the neglect of the gradient-drift instability may also be an important factor.

4. CONCLUSIONS

Our comparison of electrojet features derived from magnetic observations with those of a physical model has given, above all, very persuasive evidence for the frequent presence of effects due to neutral air winds. The wind effects appear to be variable from day to day and throughout the course of an individual day. Around midday, there is strong evidence that high-altitude westward winds usually tend to augment $S_R^P(H)$ over model values which utilize a pure electric field, and often tend to produce the appearance of a second, wider ribbon of current, oppositely directed to the main ribbon. This secondary ribbon is not actually an independent additional current around the equator, but rather a deficit in the wind-produced augmentation of the large-scale planetary current component in the equatorial region.

The influence of plasma instabilities on the currents is less clear than the influence of winds. The observations suggest that the electrojet may be widened and its intensity reduced by instabilities in qualitative but not quantitative agreement with the model. Although winds could conceivably account for the quantitative discrepancies, we feel that part of the discrepancies, in particular the model's consistent underestimation of the electrojet width, may well be explained by an important influence of the gradient-drift instability, which the model neglects.

Finally, if anything, this paper points to the need for simultaneous measurements of the magnetic field, plasma drift velocities, and ionospheric winds in the equatorial region.

Acknowledgement—A. D. Richmond was supported by a NATO Postdoctoral Fellowship in Science.

REFERENCES

Bedinger J. F. 1972 *Space Research XII*, p. 919. Akademie-Verlag, Berlin.
Fambitakoye O. 1974 Doctoral thesis, University of Paris VI.
Fambitakoye O. and Mayaud P. N. 1976a *J. atmos. terr. Phys.* **38**, 1.
Fambitakoye O. and Mayaud P. N. 1976b *J. atmos. terr. Phys.* **38**, 19.
Hutton R. 1967 *J. atmos. terr. Phys.* **29**, 1411.
Kochanski A. 1964 *J. geophys. Res.* **69**, 3651.
Maynard N. C. 1967 *J. geophys. Res.* **72**, 1863.
Olson W. P. 1970 *J. geophys. Res.* **75**, 7244.
Richmond A. D. 1973a *J. atmos. terr. Phys.* **35**, 1083.
Richmond A. D. 1973b *J. atmos. terr. Phys.* **35**, 1105.
Rogister A. 1971 *J. geophys. Res.* **76**, 7754.
Rosenberg N. W. 1968 *J. atmos. terr. Phys.* **30**, 907.
Sato T. 1972 *Phys. Rev. Lett.* **28**, 732.
Sato T. 1974 *Phys. Fluids* **17**, 621.
Stening R. J. 1969 *J. atmos. terr. Phys.* **31**, 849.
Woodman R. F. 1972 *Space Research XII*, p. 969. Akademie-Verlag, Berlin.

Journal of Atmospheric and Terrestrial Physics, Vol. 38, pp. 123 to 134. Pergamon Press, 1975. Printed in Northern Ireland

Equatorial electrojet and regular daily variation S_R—IV. Special features in particular days

O. FAMBITAKOYE
S.S.C.-ORSTOM 93, Bondy, France

and

P. N. MAYAUD*
Institut de Physique du Globe, Université Paris VI, France

(*Received* 26 *March* 1975)

Abstract—Special features of the regular daily variation S_R in the region of the equatorial electrojet are set forth from magnetic H and Z profiles for each local hour of particular days. It is pointed out that afternoon low-latitude negative disturbances in H are not amplified along the dip equator whereas irregular fluctuations are amplified and tend to inhibit the variation S_R. Examples of the day-to-day variability are displayed for consecutive days; some of them can be related to the presence of a counter-electrojet, others to the effect of neutral winds. Finally, strong counter electrojet events are discussed.

1. INTRODUCTION

In the last paper of a series concerning the regular daily variation S_R in the region of the equatorial electrojet (FAMBITAKOYE and MAYAUD, 1975, a, b; FAMBITAKOYE *et al.*, 1975; hereinafter called papers I, II and III), we present latitudinal H and Z profiles of this variation for each daytime hour of particular days. These days are chosen in a series of 171 days (FAMBITAKOYE, 1974) in order to display special features (disturbance effects, day-to-day variability, counter-electrojet). We suggest an explanation for some of them; we only attempt to set forth the question raised by others.

In paper I, we described the analysis method by which the variation S_R is split up into two components: the $S_R{}^P$ which corresponds to the magnetic effects of the confluence (or divergence), at low latitudes, of current lines of the planetary vortices, and the $S_R{}^E$ which corresponds to the magnetic effects of the supplement of currents flowing in a narrow latitude band along the dip equator. According to paper III, these components are equivalent to the height-integrated 'background current density' and to the height-integrated 'electrojet enhancement current density' of RICHMOND (1973), both current densities being due to the primary eastward (or westward) electric field E_ϕ. Furthermore, eastward (or westward) neutral winds v_ϕ bring about magnetic effects easy to identify.

In the profiles displayed hereafter (see, for instance, Fig. 1), the variation $S_R{}^P$ which is drawn results from the analysis; the variation $S_R{}^E$ would be equal to the difference $S_R - S_R{}^P$.

2. SOME DISTURBANCE EFFECTS

2.1. *Effect on the zero level*

On 28 May 1969 (see Fig. 1), there exists a weak activity. The $S_R{}^P(H, c)$ amplitude at the centre c is small ($\sim$25 γ) relatively to that of the adjacent quiet days ($>$50 γ). Furthermore, the $S_R{}^P$ becomes negative all along the profile from 1530 h ($-5\,\gamma$) to 1730 h ($-15\,\gamma$). The $S_R{}^E$ (H, c) is small at midday ($\sim$20 γ) and maximized at 1430 h (42 γ) although the $S_R{}^P$ is much smaller than at midday.

The question raised by this example is as follows: why do the shape of the H and Z profiles correspond in the late afternoon to an eastward electrojet while the $S_R{}^P$ (H, c) is negative (apparent westward planetary currents)? The analysis results in a half-width of 450 km at 1630 h, which is characteristic of the normal width of the equatorial electrojet over Central Africa (see, paper I, Fig. 11); this fact confirms that the normal electrojet is present at that time of the day and should be fed by an eastward 'background' current.

The cause of the apparent discrepancy is a disturbance associated with an auroral event. A

* Contribution I.P.G. N° 144.

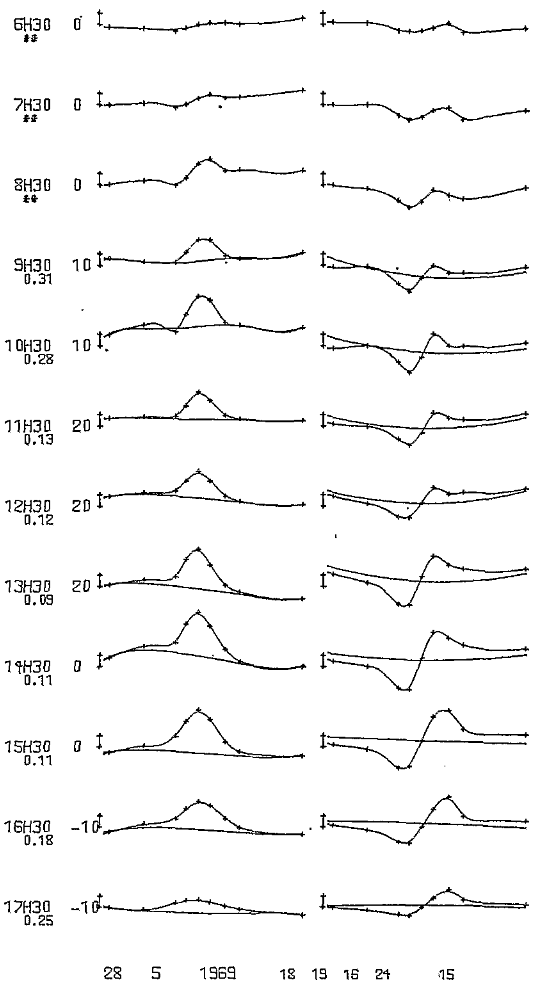

Fig. 1. Example of the effect of a low-latitude negative disturbance in H. (Crosses indicate observed values S_R—adjusted to 15°E time—at the nine stations of the profile. Curves of the left column, drawn through the crosses, display the S_R latitudinal profiles in H at a given local hour; curves of the right column display those in Z. Below each time is a number giving the relative size of the residues of the analysis, provided that this number is not greater than 0·40—see paper I. The supplementary curves drawn in these cases display the $S_R{}^P$ in each component. The vertical bars to the left of each profile represent 10γ; for the Z profiles, the horizontal mark at the bar represents the base level, while for the H profiles this mark represents a value either $0\,\gamma$, $10\,\gamma$, $20\,\gamma$ . . . (or $-10\,\gamma$ . . .) above (or below) the base level, as indicated to the left. The distance between extreme stations is 3020 km; the north is to the left, and the dip equator is close to the central station. At the bottom are given the date, the a_m index values for the four 3-h intervals from 0600 h to 1800 h UT, and the average a_m value for the 24 h day).

comparison of the records of Bangui and M'Bour (2 h apart in longitude) shows that a negative perturbation occurs in the afternoon and ends at 1800 UT at both stations (see MAYAUD, 1967, about the universal time dependency of such perturbations). At Tromsö, a high-latitude station of similar longitude, an eastward auroral electrojet ($\sim 140\,\gamma$) occurs during the afternoon. Now, the zero level does not take that perturbation into account, and the deviations scaled from this level include effects of the perturbation. Then, the S_R is contaminated in H by the negative disturbance in the afternoon. Two remarks can be made concerning the zero level method and the region where the currents are flowing.

(1) We defined the zero level (see paper I, Section 2) by an assumed 'linear variation' between two 'nocturnal' moments (around 0200 h LT) which are assumed to be 'free of any disturbance or S_R effect.' The single reliable assumption is probably that the amplitude of the S_R variation is null at the chosen moments. As for the others, disturbances (especially in H at low latitudes) can be always present at any time during quiet days; they alter the zero level at the 'nocturnal' moments chosen as a reference, and they prevent the assumed 'linear variation' to be truly linear. Usually, disturbances are small (a few gammas) during quiet days and they can be positive or negative. But a special class, the late afternoon disturbances associated with an auroral event, are always negative and can be large (a few tens of gammas, even during quiet days). Their identification, and elimination is extremely difficult (see MAYAUD, 1967, Fig. 41 for an example during a quiet day). Consequently any quantitative comparison between $S_R{}^P$ and $S_R{}^E$ during the afternoon hours is subject to this source of error as long as a careful examination of the records does not permit one to assert that no auroral event is present at neighbouring longitudes.

(2) Given the amplitudes observed for the $S_R{}^E(H, c)$ and $S_R{}^P(H, c)$ at 1530 h on 28 May 1969 (see Fig. 1: $+41\,\gamma$ and $-5\,\gamma$ respectively), it is clear that the $S_R{}^E$ is fed by actual eastward $S_R{}^P$ currents whose magnetic positive effects are masked by the negative perturbation and that the latter is insensitive to any equatorial electrojet enhancement. This fact strongly suggests that the negative perturbation is not caused by currents flowing in the lower ionosphere. Many workers in the recent years have pointed out that such low-latitude negative disturbances are not the ionospheric closure of the ionospheric auroral electrojet. KAMIDE and FUKUSHIMA (1972) or CROOKER and MCPHERRON

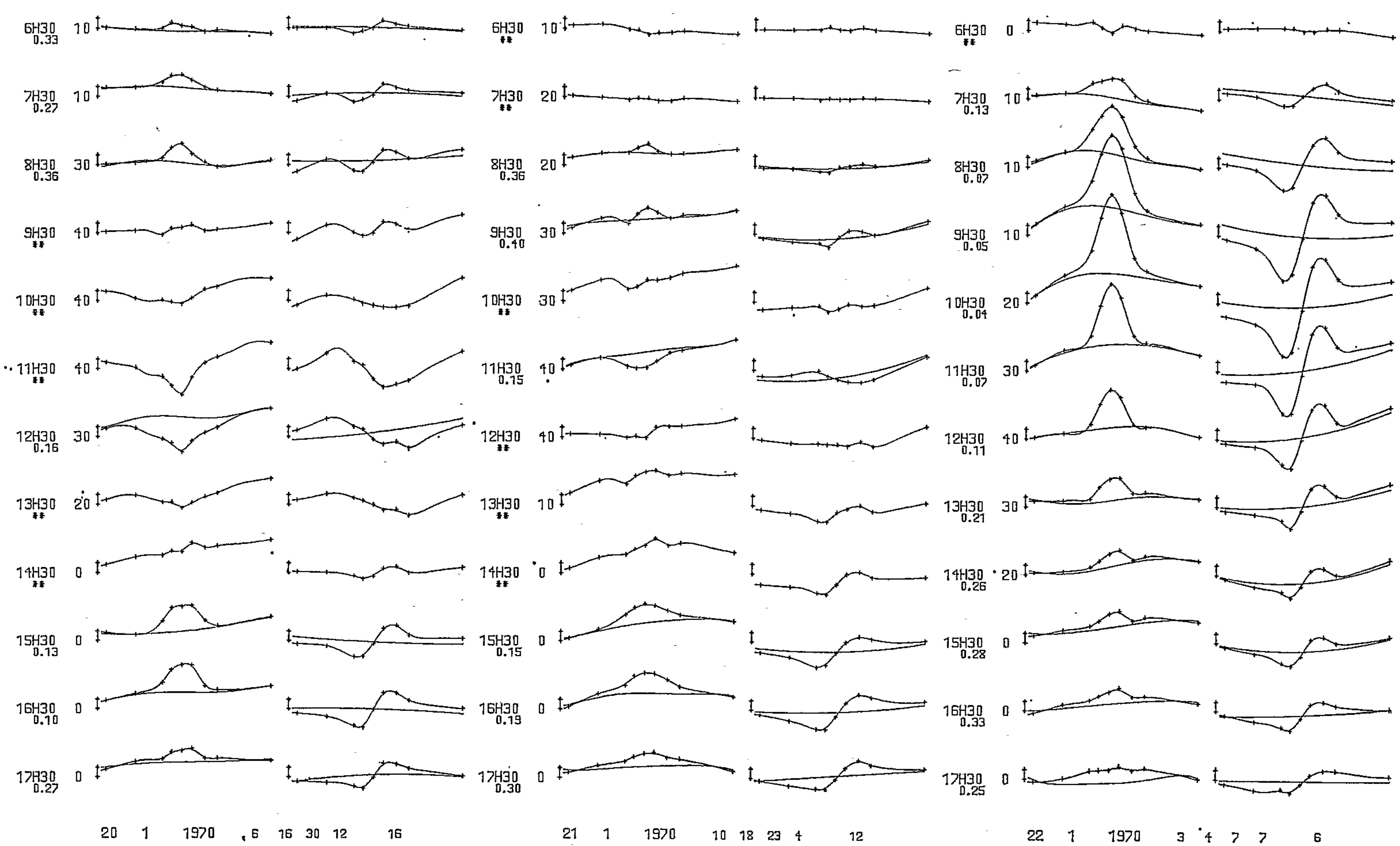

Fig. 2. Example of the effect of irregular fluctuation (see caption to Fig. 1).

(1972) suggest that they are due to a partial ring current whose eastward auroral electrojet would be the ionospheric closure. The absence of equatorial enhancement of such disturbances (as it is for the main phase of the storms) is consistent with this interpretation.

2.2. *Effect of the irregular fluctuations*

Figure 2 displays a sequence of three consecutive days of which the third only is very quiet. From 0830 to 1430 h, the S_R^E is nearly erased on the 20 and the 21 January (there exists a net reversal of the H and Z profiles at 1130 and 1230 on the 20 January) whereas it is strongly developed on the 22 January. However, the S_R^P (H, c) has the same amplitude (40–50 γ) at midday hours. Figure 3 gives the H-magnetograms for the 20 and the 22 January at two stations: S_5, the central station (very close to the dip equator), and S_2 (the second station from the left hand of the profiles), a station at which the electrojet effects in H are small (see the morning H profiles on the 22 January in Fig. 2). Whereas S_2 and S_5 records are almost identical on the 20 January at night-time (see, in particular, around 2100 h), they greatly differ at daytime: (1) irregular fluctuations* exist at S_5, they can hardly be seen at S_2; (2) a secondary minimum exists in variation S_R at S_5, it hardly appears at S_2 (there exists a constant level between 0900 h and 1200 h). Then the question is the following: what is the reason for the radically different behaviour of the equatorial electrojet phenomenon on the 20 and on the 22 January?

First of all, the S_R (H, c) is never negative on the 20 January *at midday hours* with respect to the zero-level chosen (see Fig. 2 or Fig. 3). Now, if H and Z profiles are clearly reversed at 1130 h and 1230 h, this is not necessarily the sign of a westward current: a deficit of the eastward currents along the dip equator (instead of an enhancement) also corresponds to reversed magnetic profiles. Westward neutral winds (see paper III) induce such a deficit. However, since the S_R (H, c) is very small, it would mean that the eastward electric field E_ϕ is itself very small; consequently, the 'background current density' is also very small, and the amplitude of the S_R observed in H at a station such as S_2 would be due only to the neutral winds. Given the half-width observed at 1230 h ($a = 1100$ km), it would suppose very strong winds blowing at very high altitudes only (see paper III, Fig. 1(a) and Fig. 2: the width increases when the lowest altitude of the wind increases). Another cause of this deficit is suggested by the following observation. Anyone looking at a long series of equatorial magnetograms is quickly impressed by a frequent decrease of the S_R amplitude when fluctuations occur, whereas the latter are greatly enhanced. This observed apparent contradiction may present some new theoretical problems. Thus one may wonder if the observed fluctuations with a few minutes time-scale modify the physics of the S_R equatorial enhancement by comparison with a near-stationary equilibrium.

2.3. *A further question*

Irregular fluctuations (SSC's, SI's, any more or less rapid move of the records) are sensitive, during day-time, to an enhancement much larger than that of the S_R itself (see Fig. 3). This well-known fact (see, e.g., Sugiura, 1953, for the SSC's; Mayaud, 1963, for all the fluctuations) contrasts with the absence of the amplitude daily variation in the fluctuations at low latitudes (see, e.g. Mayaud, 1975, where about 2300 SSC's were studied for one low latitude station). The latter observation is

* The irregularity of the profiles at midday hours on the 20 January, which contrasts with their regularity on the 22 January, is due to the greater agitation.

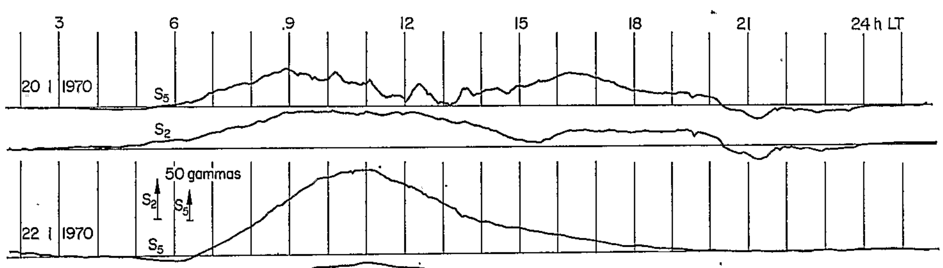

Fig. 3. Normal H magnetograms at stations S_2 and S_5 on 20 and 22 January 1970. Zero levels are indicated by the lines joining one night to another.

consistent with the generally held view that SSC's are mainly the effects of a compression of the magnetosphere and that they are not the effects of currents generated by electric fields in the ionosphere. However, SUGIURA (1971) pointed out that a compressional hydromagnetic wave propagating downwards into the ionosphere will create a polarization electric field at the wave front as the wave hits the dynamo layer (where the Hall conductivity is large) due to the ion drag and that the Hall current from the polarization field gives rise to the negative impulse in a SSC in the equatorial region during the sunlit hours; the main variation in an SSC is also amplified in the equatorial region due to an enhanced Hall current associated with the compressional wave. Thus, we know that compressional disturbances (SC) in the solar wind generate, at the magnetopause, compressional hydromagnetic modes, which can stimulate the electrojet when they propagate to earth.

In addition, CORONITI and KENNEL (1973) have suggested that changes in solar wind magnetic field direction stimulate torsional and slow hydromagnetic waves at the magnetopause. Whether these interact effectively with the electrojet is not known. At any rate, measurements of electric fields by MOZER (1971) and CARPENTER (1972) indicate that external electric field fluctuations can be imposed upon the ionosphere. Again, what effects these have upon the equatorial electrojet is not known with precision. However, it seems to us that understanding of the amplification of short-period fluctuations in the electrojet may come from a study of the coupling between the equatorial electrojet and magnetospheric electric field fluctuations.

3. DAY-TO-DAY VARIABILITY

Figure 4 displays the profiles of two consecutive days which are very quiet. S_R^E profiles are very similar in both days during the early morning. Differences intervene from 0930 h onwards and become very large from 1130 h to 1430 h. The analysis detects a secondary ribbon from 1130 h to 1530 h on the 22 September, only at 1530 h on the 21 September. The shapes of the profiles are typical of wind effects (see paper III) and it is certain that the variability from one day to another, in that case, is due to stronger winds on the 22 September.

Another feature is of importance; the strong asymmetry (with respect to the dip equator) in the intensity of the S_R^P in H from 0830 h to 1130 h on the second day of Fig. 4. Such a fact is not rare in our series of profiles and could be partly attributed to neutral winds varying with latitude. The sense of the asymmetry can be reversed, but the configuration occurring on this day is more frequent.

Figure 5 displays the profiles of two other consecutive days, the first of which is quiet and the second very quiet (note that they belong to the series of days whose electrojet parameters are given in paper I, Fig. 13). At midday hours, the S_R^E amplitude is twice as small on the 8 July as on the 7 July, whereas the S_R^P amplitude H is nearly the same. Table 1 which gives the current densities $I_{0,1}$ (main ribbon) and $I_{0,2}$ (secondary ribbon) at the centre c, as resulting from the analysis, indicates that the difference is partly due to neutral winds at 1230 h and 1330 h. Thus, at 1330 h, values of $I_{0,1}$ are similar in both days. But why are they so different at 1030 h and 1130 h? The two days clearly differ in the early morning: a counter-electrojet exists on the 8 July whereas no such phenomenon appears on the 7 July. Then, a possible assumption is that the counter-electrojet would be active up to 1230 h on the 8 July and superimposed upon the eastward electrojet (in Fig. 13 of paper I, days where the ratio R_q is the smallest at midday hours are those for which a stronger counter-electrojet exists in the early morning—compare, for instance, the 2nd and the 3rd on this Figure). Because the widths of both the electrojet and the counter-electrojet would be nearly equivalent, the shape of the profiles is not deformed when the electrojet intensity is larger than that of the counter-electrojet, but the apparent S_R^E amplitude is greatly reduced. Such a fact would be confirmed by the statistical observations of GOUIN and MAYAUD (1967) and MAYAUD (1967): the average amplitude of the S_R at Addis-Ababa is abnormally small at midday hours when compared to those of other electrojet stations, and this fact can be related to the larger amplitude of the morning counter-electrojet at Addis-Ababa.

Figure 6 gives a last, and anomalous, example of the day-to-day variability. Both days are quiet and small irregular fluctuations have the same average amplitude. Now, the S_R^E appears to be almost entirely non-existent on the 30 June. The S_R profiles are rather ill-shaped and look as if an unstable phenomenon were in progress. Such an example is nearly *unique* in our series of observations and is very hard to understand. One can note that the day-to-day variability is just as large in the S_R^P at midday hours: its amplitude in H is twice as large on the 30 June as on the 29 June.

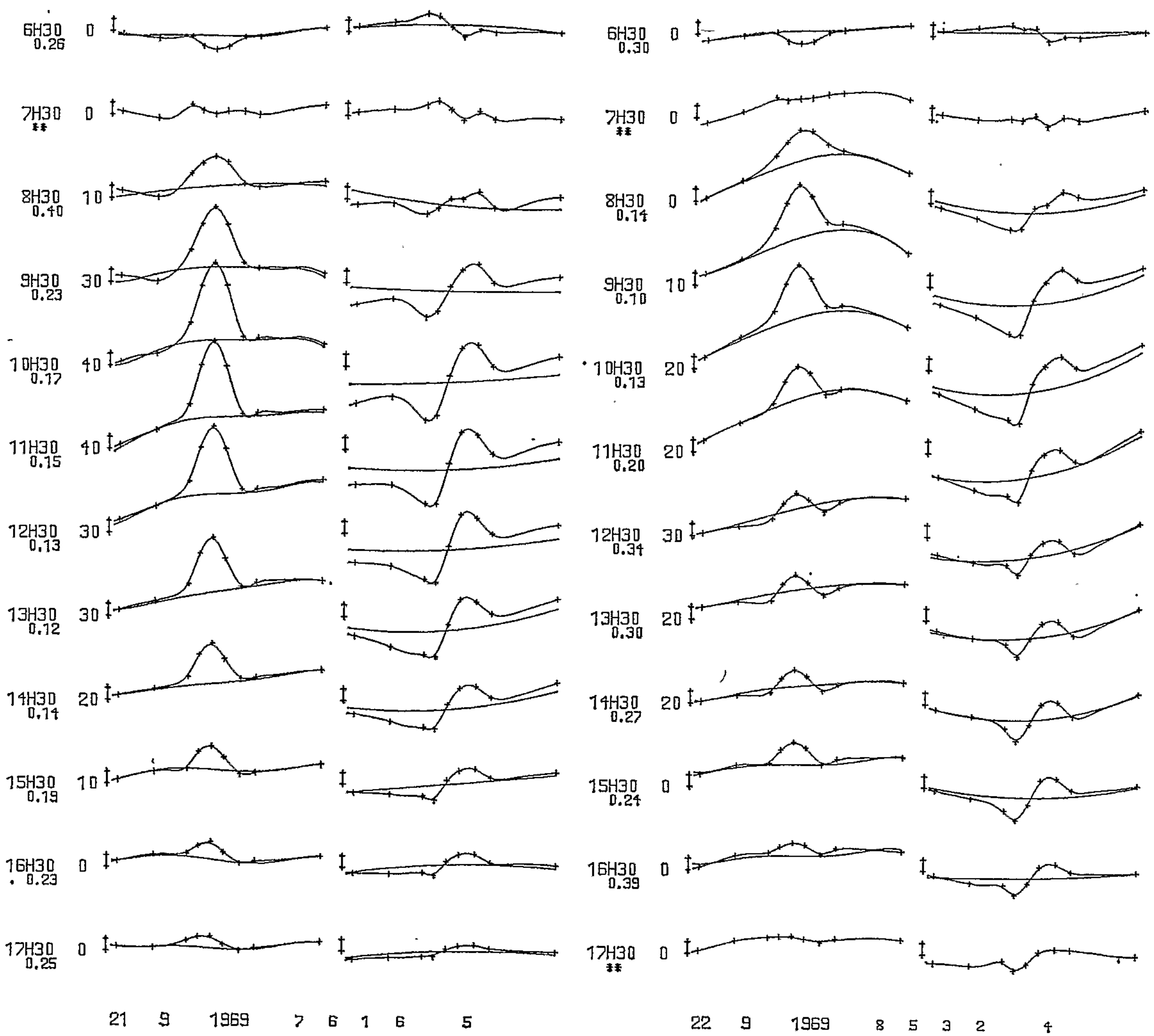

Fig. 4. Example of a day-to-day variability of the S_R, due to the variability of the winds (see caption to Fig. 1).

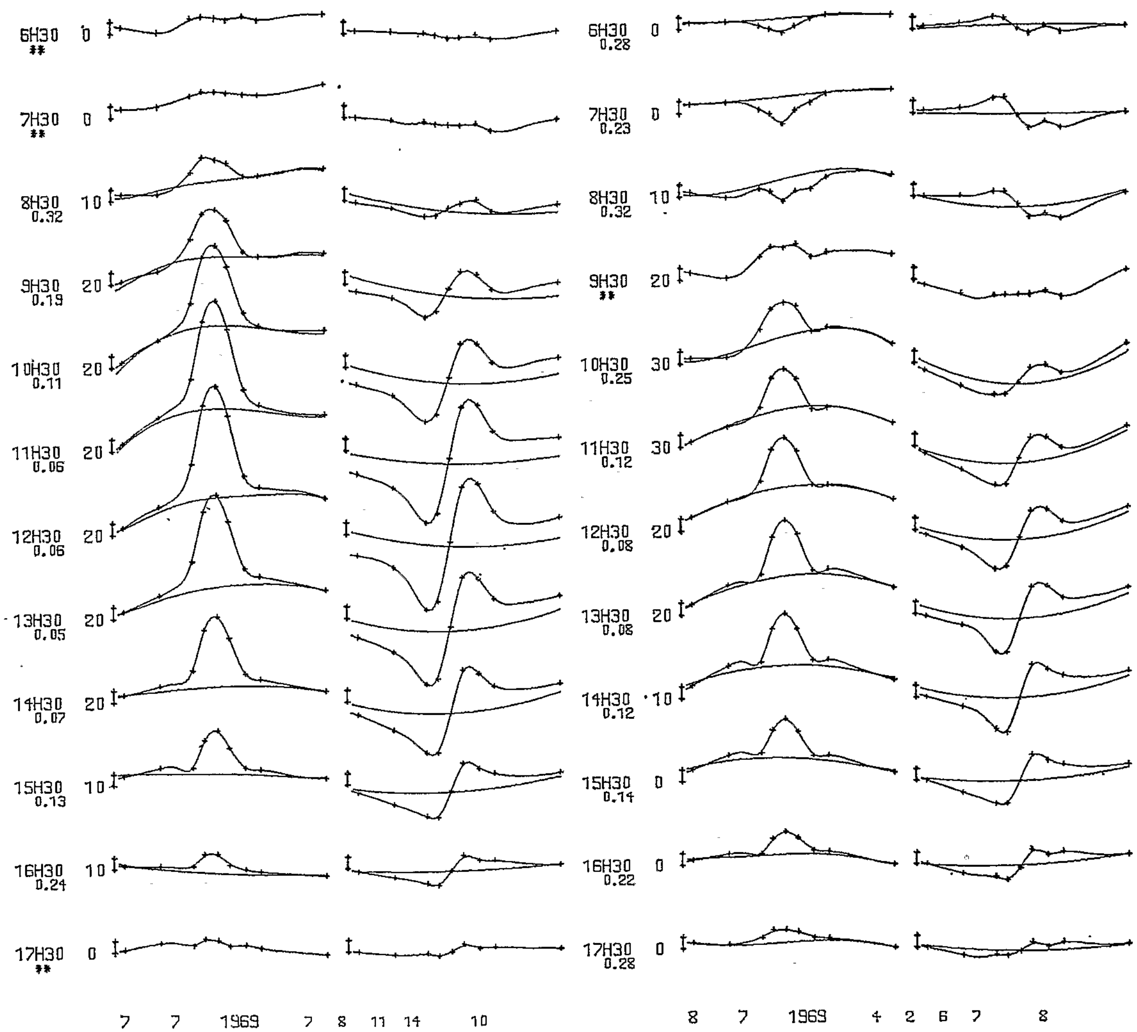

Fig. 5. Example of a day-to-day variability, possibly due to the permanence of a counter-electrojet on the second day (see caption to Fig. 1).

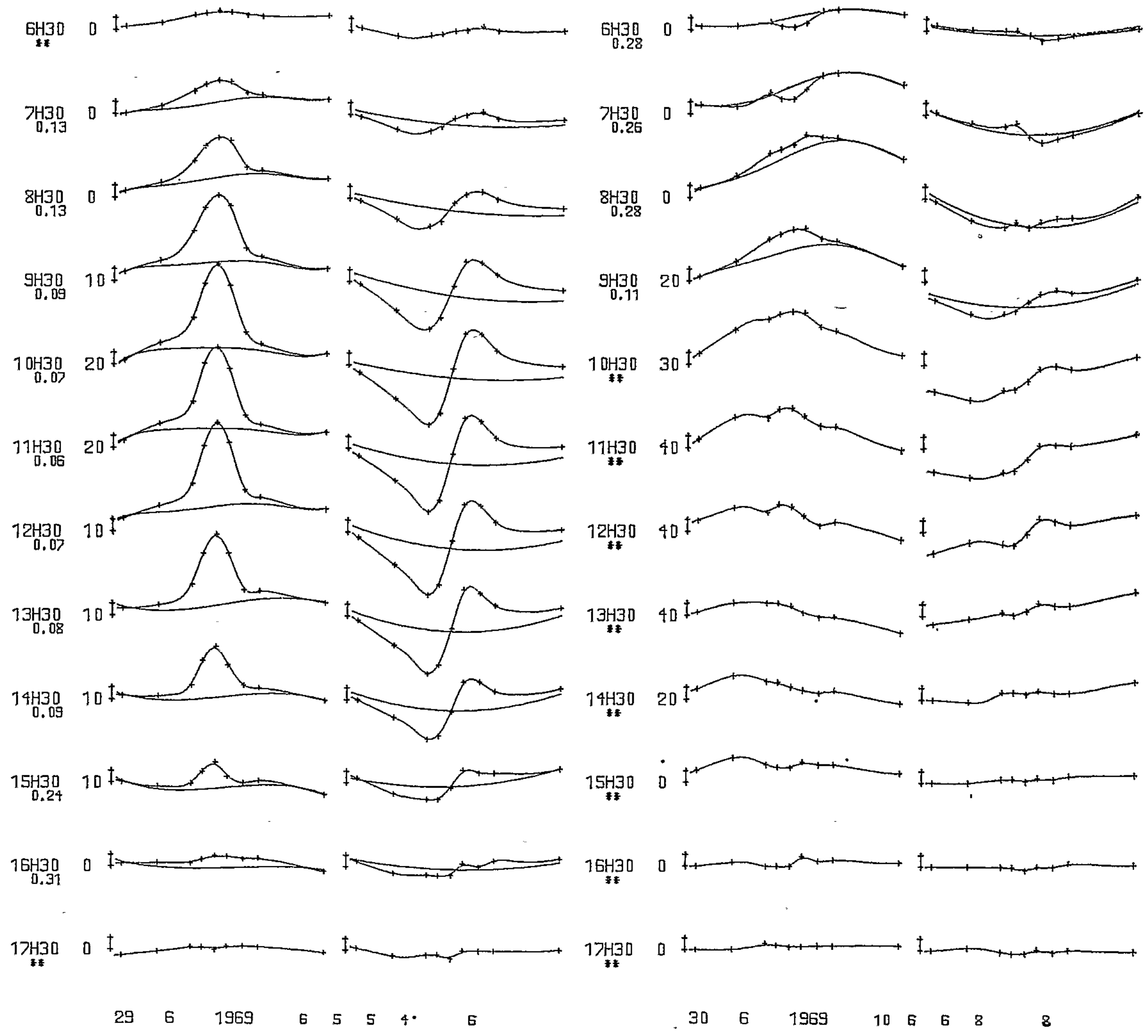

Fig. 6. Example of an anomalous behaviour of the electrojet on a quiet day (30 June 1969) and comparison with the preceding day (see caption to Fig. 1).

Table 1.

		1030 h	1130 h	1230 h	1330 h
7/7/1969	$I_{0,1}$	148	205	219	187
	$I_{0,2}$	—	—	—	—
8/7/1969	$I_{0,1}$	58	95	116	160
	$I_{0,2}$	—	−17	−21	−46

Current densities (amp/km) at the centre (a(—) means that no secondary ribbon is detected).

4. THE COUNTER-ELECTROJET

Figures 7 and 8 display examples of strong counter-electrojets either in the morning or in the afternoon (the second day of Fig. 8 belongs to the series of seven consecutive days whose electrojet parameters are given in paper I, Fig. 13). These examples are chosen among the days during which such a phenomenon is strongest, and belong to both solstices.

Table 2 gives values of S_R^P (H, c) and S_R (H, c) at hours when the counter-electrojet (reversed profiles) is present and when the analysis does not fail. They clearly demonstrate that the S_R (and *a fortiori* the $S_R^E = S_R - S_R^P$) is negative whereas the S_R^P is positive. The half-widths are about 450 km for the morning cases, between 400 and 600 km for the afternoon cases. Then a westward ribbon of currents, whose width is similar to that of the normal electrojet, is certainly flowing at these hours along the dip equator whereas the 'background current density' is still eastwards. A strong disconnection between S_R^P and S_R^E such as that mentioned in paper I appears in these cases. We would like to suggest the following assumption: (1) The S_R^P is made up of two components at such times, one corresponding to a background eastward current flow, and the other, smaller (since the S_R^P is positive), to a background westward flow. (2) Since the S_R^E observed appears as being the magnetic effects of a westward ribbon, the enhancement at equatorial latitudes would be much larger for the background westward flow. Recall that the observation of FAMBITAKOYE *et al.* (1973) concerning the disappearance of the *Esq* type traces from ionograms at the time of the counter-electrojet would indicate that westward currents flow at the bottom of the ionospheric E-layers.

5. CONCLUSION

The examples given are sometimes extreme cases (in particular Fig. 6). They permit one to understand better the great dispersion of the points in Figs. 5 and 6 of paper III. However such a variability must not lead one to conclude that S_R^E and S_R^P are independent phenomena. One may say that three main factors contribute to the S_R^E variability and are added to the variability of the planetary vortices:

(1) the agitation tends to diminish the enhancement of the regular daily variation,

(2) neutral winds introduce more or less large deformations of the profiles,

(3) the counter-electrojet occurs more or less frequently, or can be superimposed upon the normal electrojet.

In addition to the problem set forth in paper III (discrepancy between the Richmond model and the observed facts concerning the width and the electrojet enhancement), some main problems still unsolved are:

(1) Why so irregular fluctuations partly inhibit the equatorial enhancement of the S_R?

(2) Why are irregular fluctuations more enhanced than the S_R?

(3) What is the origin of the counter-electrojet?

(4) What is the cause of the difference between the almost regular occurrence of the morning counter-electrojet and the extremely fugacious occurrence of the afternoon counter-electrojet events?

No solution can be given by magnetic ground-data only. It would need large interdisciplinary cooperation. In a first step, high altitude resolution coherent radar experiments working in latitudinal and longitudinal diversity would permit one

Table 2

	6/6/1969				28/12/1968	
	0630 h	0730 h	0830 h	0930 h	0630 h	0730 h
S_R^P	14·2	27·7	42·7	61·9	−1·3	9·4
S_R	−12·2	−32·1	−13·9	18·2	−30·3	−24·0

	15/7/1969			10/1/1970			
	1430 h	1530 h	1630 h	1330 h	1430 h	1530 h	1630 h
S_R^P	34·6	20·5	16·4	25·5	13·1	12·1	12·6
S_R	4·1	−13·2	−5·4	−3·9	−29·0	−24·8	−1·4

Values (in gammas) of $S_R^P(H, c)$ and $S_R(H, c)$ at the centre of the profile.

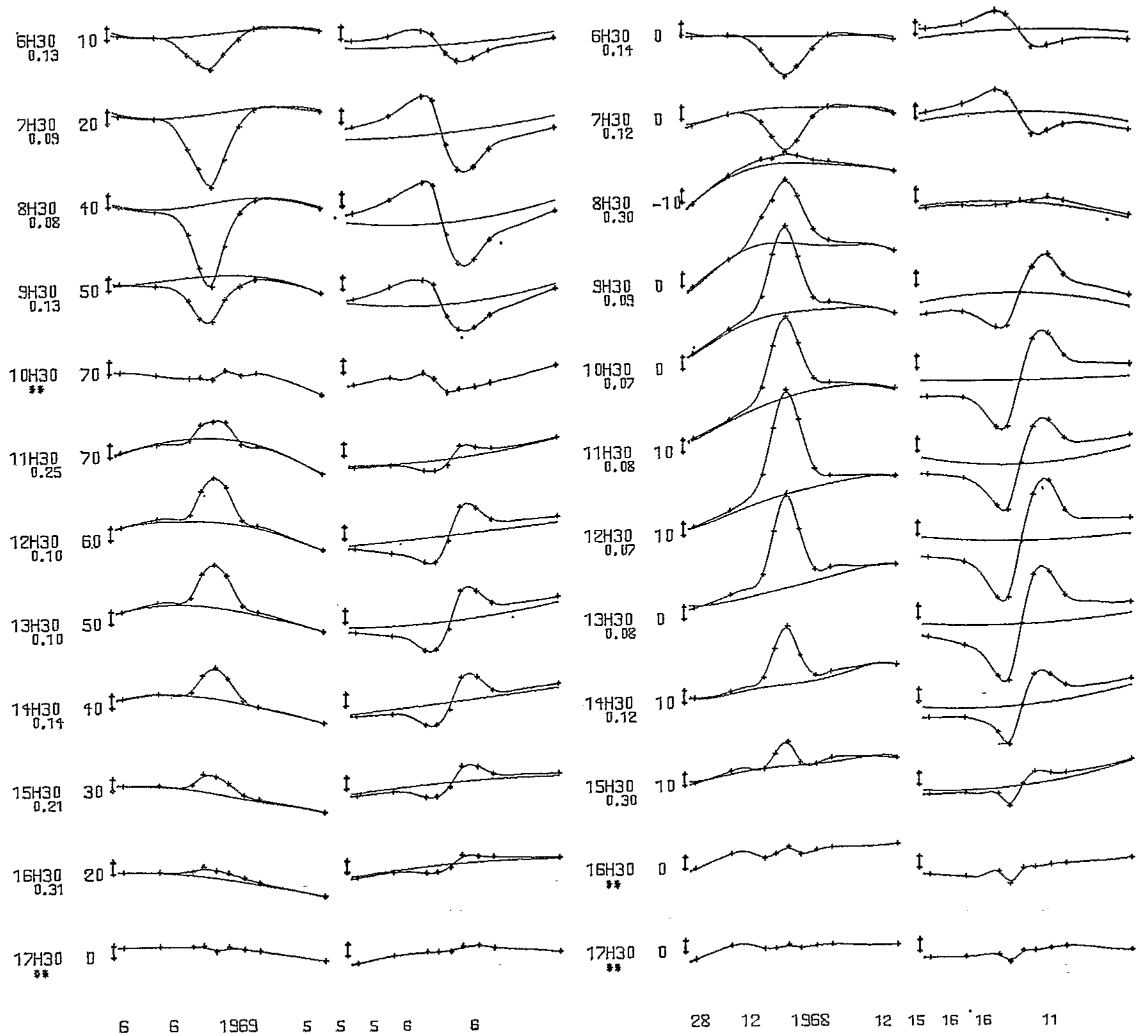

Fig. 7. Example of morning counter-electrojet at both solstices (see caption to Fig. 1).

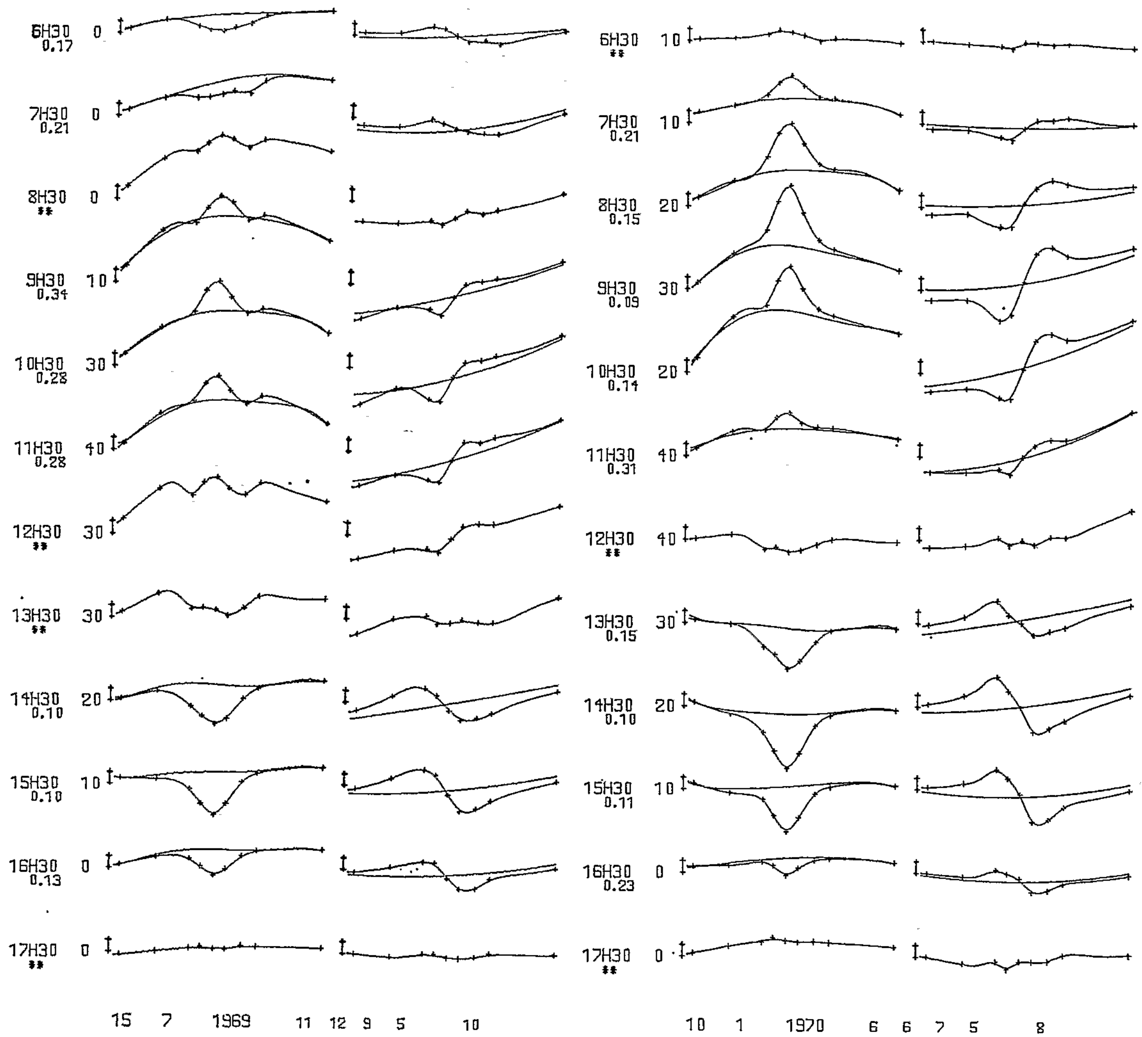

Fig. 8. Example of afternoon counter-electrojet at both solstices (see caption to Fig. 1).

to obtain information on the physical conditions existing in equatorial ionosphere. In a second, and more difficult step, one would have to improve knowledge concerning the planetary variability of the S_R and to understand what part of it gives rise to the counter-electrojet.

Acknowledgements—The authors thank the Directors of Binza and Tamanrasset observatories for providing their magnetograms. Other data used in this study have been acquired with the support of Recherche Coopérative sur Programme (RCP 168) of the C.N.R.S. The authors also thank Drs. KENNEL and SUGIURA for their advice concerning the contents of Section 2.3.

REFERENCES

CARPENTER D. L. *et al.* 1972 *J. geophys. Res.* **77**, 2819.
CROOKER N. M. and MCPHERRON R. L. 1972 *J. geophys. Res.* **77**, 6886.
FAMBITAKOYE O., RASTOGI R. G., TABBAGH J. and VILA P. 1973 *J. atmos. terr. Phys.* **35**, 1119.
FAMBITAKOYE O. and MAYAUD P. N. 1976a *J. atmos. terr. Phys.* **38**, 1,
FAMBITAKOYE O. and MAYAUD P. N. 1976b *J. atmos. terr. Phys.* **38**, 19.
FAMBITAKOYE O., MAYAUD P. N. and RICHMOND A. D. 1976 *J. atmos. terr. Phys.* **38**, 113.
GOUIN P. and MAYAUD P. N. 1967 *Annls Géophys.* **23**, 41.
KAMIDE Y. and FUKUSHIMA N. 1972 *Rept. Ionos. Space Res., Japan* **26**, 79.
MAYAUD P. N. 1963 *Annls Géophys.* **19**, 164.
MAYAUD P. N. 1967a IAGA Bulletin 21, I.U.G.G. Publication Office, Paris.
MAYAUD P. N. 1967b *Annls Géophys.* **23**, 387.
MAYAUD P. N. 1975 *J. geophys. Res.* **80**, 111.
MOZER F. S. 1971 *J. geophys. Res.* **76**, 3651.
RICHMOND A. D. 1973 *J. atmos. terr. Phys.* **35**, 1083.
SUGIURA M. 1953 *J. geophys. Res.* **58**, 858.

Reference is also made to the following unpublished material:

FAMBITAKOYE O. 1974 Thèse de Doctorat d'Etat, Paris VI.
SUGIURA M. 1971 Communication to the XVth IUGG General Assembly, IAGA Abstracts, p. 369.